Caffeine intake exerts dual genome-wide effects on hippocampal metabolism and learning-dependent transcription

Isabel Paiva[1†], Lucrezia Cellai[2,3†], Céline Meriaux[2,3†], Lauranne Poncelet[4†], Ouada Nebie[2,3], Jean-Michel Saliou[5], Anne-Sophie-Lacoste[5], Anthony Papegaey[2,3], Hervé Drobecq[6], Stéphanie Le Gras[7], Marion Schneider[8], Enas M. Malik[8], Christa E. Müller[8], Emilie Faivre[2,3], Kevin Carvalho[2,3], Victoria Gomez-Murcia[2,3], Didier Vieau[2,3], Bryan Thiroux[2,3], Sabiha Eddarkaoui[2,3], Thibaud Lebouvier[2,3,9], Estelle Schueller[1], Laura Tzeplaeff[1], Iris Grgurina[1], Jonathan Seguin[1], Jonathan Stauber[4], Luisa V. Lopes[10], Luc Buée[2,3], Valérie Buée-Scherrer[2,3], Rodrigo A. Cunha[11,12], Rima Ait-Belkacem[4‡], Nicolas Sergeant[2,3‡], Jean-Sébastien Annicotte[13,14‡], Anne-Laurence Boutillier[1‡*], David Blum[2,3‡*]

† Equal contributions
‡ Equal contributions

1. University of Strasbourg, CNRS, UMR7364 - Laboratoire de Neuroscience Cognitives et Adaptatives (LNCA), F-67000 Strasbourg, France.
2. University of Lille, Inserm, CHU Lille, UMR-S1172 LilNCog - Lille Neuroscience & Cognition, Lille, France.
3. Alzheimer and Tauopathies, LabEx DISTALZ, France.
4. ImaBiotech SAS, Parc Eurasanté, F-59120 Loos, France.
5. Univ. Lille, CNRS, Inserm, CHU Lille, Institut Pasteur de Lille, UAR CNRS 2014 - US Inserm 41 - PLBS, F-59000 Lille, France
6. CIIL - Centre d'Infection et d'Immunité de Lille (CIIL) - INSERM U1019 - UMR 9017
7. Univ. Strasbourg, CNRS UMR7104, Inserm U1258 - GenomEast Platform – IGBMC - Institut de Génétique et de Biologie Moléculaire et Cellulaire, F-67404 Illkirch, France.
8. PharmaCenter Bonn, Pharmaceutical Institute, Pharmaceutical & Medicinal Chemistry, University of Bonn, D-53121 Bonn, Germany.
9. CHU Lille, Memory Clinic, Lille France.
10. Instituto de Medicina Molecular, Faculdade de Medicina de Lisboa, Universidade de Lisboa, Lisbon, Portugal.
11. CNC - Center for Neuroscience and Cell Biology, University of Coimbra, 3004-504 Coimbra, Portugal.
12. Faculty of Medicine, University of Coimbra, 3004-504 Coimbra, Portugal.
13. Univ. Lille, INSERM, CNRS, CHU Lille, Institut Pasteur de Lille, Inserm U1283 / CNRS UMR8199 - EGID, 59000 Lille, France.
14. Univ. Lille, INSERM, CHU Lille, Institut Pasteur de Lille, U1167 – RID-AGE-Facteurs de risque et déterminants moléculaires des maladies liées au vieillissement, 59000 Lille, France.

[#] Correspondence to:
David Blum, Inserm UMR-S1172, "Alzheimer & Tauopathies", Place de Verdun, 59045, Lille Cedex, France. Orcid Number: 0000-0001-5691-431X. Tel: +33320298850, Fax: +33320538562. david.blum@inserm.fr
Anne-Laurence Boutillier, Laboratoire de Neuroscience Cognitives et Adaptatives (LNCA), UMR7364 Cnrs Unistra, 67000 Strasbourg, France. Orcid Number: 0000-0002-2317-928.0 laurette@unistra.fr

Conflict of interest. The authors have declared that no conflict of interest exists.

Abstract

Caffeine is the most consumed psychoactive substance worldwide. Strikingly, molecular pathways engaged by its regular consumption remain unclear. We herein addressed the mechanisms associated with habitual (chronic) caffeine consumption in the mouse hippocampus using untargeted orthogonal-omics techniques. Our results revealed that chronic caffeine exerts concerted pleiotropic effects in the hippocampus, at the epigenomic, proteomic and metabolomic levels. Caffeine lowers metabolic-related processes in the bulk tissue, while it induces neuronal-specific epigenetic changes at synaptic transmission/plasticity-related genes and increased experience-driven transcriptional activity. Altogether, these findings suggest that regular caffeine intake improves the signal-to-noise ratio during information encoding, in part through a fine-tuning of metabolic genes while boosting the salience of information processing during learning in neuronal circuits.

Introduction

Caffeine is the most consumed psychoactive substance worldwide (about 80% of the population) via dietary intake from coffee, tea and soda beverages. Its popularity derives from its ability to enhance well-being and some central-related functions such as attention and alertness (1). Large epidemiological studies point out an inverse association between coffee/caffeine consumption and all-cause mortality (2–4). In general, the impact of caffeine on human health follows an inverted bell-shaped dose-response curve with benefits observable at doses of 200-400 mg *per* day, that can be recapitulated by 0.3 g/L p.o. in rodents.

Compelling epidemiological and experimental evidence support that habitual/chronic caffeine consumption normalizes synaptic plasticity and cognitive decline in altered allostatic situations such as ageing, Alzheimer's disease or other neuro-psychiatric conditions (5–7). A more limited number of studies however also support that, independently of its ability to favor arousal and attention, caffeine may exhibit cognitive-enhancing properties. After being rewarded with caffeine, honeybees are able to remember a previously learned floral scent (8). Also, acute caffeine administration in rats can enhance memory test performance (9, 10). In Humans, caffeine intake immediately following learning improves discrimination performance 24 hours later (11). These results are in line with observations supporting the ability of caffeine to modulate hippocampal/cortical excitability in homeostatic conditions. Indeed, caffeine treatment in hippocampal slices enhances basal synaptic transmission (12–14) and modulates long-term potentiation (LTP) in rodents' hippocampus (12, 15, 16) and sharp wave ripple complexes, that are proposed to underlie memory consolidation (17). Caffeine also controls neuronal excitability and LTP-like effects in the human cortex (18, 19). Most of these studies however rely on acute administrations with limited relevance towards habitual/chronic consumption.

Despite caffeine's popularity, brain molecular changes associated with its chronic intake remain ill-defined. Caffeine is known to essentially interfere with the adenosinergic system where it acts as an

antagonist (20). However, adaptive downstream pathways engaged by habitual/chronic caffeine consumption have been largely overlooked. In the present study, we used a combination of unbiased orthogonal-omics techniques to analyze the epigenome, transcriptome, proteome and metabolome of the mouse hippocampus in order to uncover the molecular pathways impacted by chronic caffeine consumption in neuronal processing during learning.

Results

Mouse monitoring and caffeine concentrations. In our experimental conditions, neither mortality nor signs of animal suffering in caffeine-treated animals were encountered. Average consumption of 0.3 g/L caffeinated water was 4.83 ± 0.15 mL/mouse/day resulting in brain caffeine concentrations of 3.6 ± 1.1 μM, corresponding to a moderate intake in Humans (20). Caffeine metabolites (paraxanthine, theobromine and theophylline) were also detected in the brain of treated mice with respective concentrations of 1.9 ± 0.4 μM, 1.8 ± 0.3 μM, and 0.10 ± 0.03 μM (n=5).

Chronic caffeine consumption decreases histone acetylation of metabolic-related genes in the hippocampus. We hypothesized that chronic caffeine consumption could affect hippocampal epigenome of mice. As caffeine is a psychostimulant, we focused on two chromatin marks associated with "active chromatin" and specific transcriptional states. Histone H3 acetylation at lysine 27 (H3K27ac) is preferentially enriched at active enhancers (21), also forming large clusters of H3K27ac-enriched enhancers known as "super-enhancers" on highly transcribed genes that are cell- or tissue-specific (22, 23). Histone H3 lysines K9 and K14 (H3K9/K14ac), on which acetylation co-occurs at many gene regulatory elements, allows to differentiate active enhancers from inactive ones and thus represents a dynamic mark accounting for stimuli dependent activation (24). Locus specific acetylation was evaluated by chromatin immunoprecipitation followed by sequencing (ChIP-seq) experiments in dorsal hippocampus of control (water) and caffeine-treated mice. A total of 2 biological replicates were performed and Principal Component Analysis (PCA) of the two histone marks was generated **(Supplemental Figure 1A,B)**. Chronic caffeine intake significantly decreased the acetylation of both histone marks at many genomic loci. H3K9/14ac was depleted in 778 genomic regions (768 genes) while only 3 were rarely identified as significantly enriched in caffeine-treated animals (FDR<1E-5) **(Figure 1A, Supplemental Table 1)**. Gene ontology analysis using Genomic

Regions Enrichment of Annotations Tool (GREAT) revealed that these acetylation-depleted regions were associated with genes involved in the regulation of metabolic processes (amide, lipids), mRNA transport, regulation of translation and dendritic spine morphogenesis and development **(Figure 1B)**. A more robust effect was observed in H3K27ac whose peaks were found decreased in 2105 genomic regions (1766 genes) and increased in only 4 genomic regions in caffeine *vs.* control mice (FDR<1E-5) **(Figure 1C, Supplemental Table 2)**. Metabolic-related pathways, such as lipid catabolic or amide metabolic processes were among the decreased peaks of both histone marks **(Figure 1B,D)**. Additionally, H3K27ac-depleted regions were significantly associated with myelin-related processes, MAP kinase, negative regulation of calcium-mediated signaling pathways, as well as heterochromatin organization **(Figure 1D)**. We also performed Kyoto Encyclopedia of Genes and Genomes (KEGG) pathway analyses and identified many processes, some of which related to cAMP-, MAP kinase, Rap1-signaling pathways and circadian entrainment for both H3K9/14 and H3K27ac depleted regions **(Figure 1E)**. Of note, the KEGG pathway database pointed out metabolic-related pathways, such as “insulin signaling”, for genes depleted in acetylation of both histone marks (**Figure 1E**) and “glucagon signaling pathway” for those associated with H3K9/14ac depleted regions (**Figure 1E**, blue bars). Those genes associated with insulin and glucagon signaling pathways were represented by protein-protein interaction network analysis (STRING), showing strong interconnectivity (**Figure 1F**, yellow and pink dots, respectively). As examples, genomic region representation of the Insulin Receptor Substrate 1 (*Irs1*) gene, which is required for insulin signaling and related spine maturation and synaptic plasticity (25) and the Glycogen Synthase Kinase 3 Beta (*Gsk3b*) gene are shown **(Figure 1G),** with significant acetylation depletion for both marks in the caffeine-treated group *versus* control (respectively left, H3K9/14ac, FDR=7.75E-05 and H3K27ac, FDR=1.82E-12; right, H3K9/14ac, FDR=2.58E-11 and H3K27ac, FDR=4.83E-05). Other regions, such as those associated with *Dusp3, Psme3* and *Mlh3* genes, did not exhibit such histone acetylation changes upon caffeine treatment, attesting for selectivity of the caffeine effect for both histone marks **(Supplemental Figure 1C).** In addition, integrated pathway analysis (IPA) applied to

common ChIP-seq data of both marks confirmed that metabolic pathways, such as insulin or IGF-1 signaling, were canonical pathways downregulated upon caffeine treatment **(Supplemental Table 3)**. Potential contributors to the caffeine effects on the epigenome were further assessed using the "upstream regulator analysis" function of IPA **(Supplemental Table 4)**. We identified in the acetylation-depleted genes, TCF7L2 (Transcription factor 7-like 2) as the most significant upstream regulator inhibited upon caffeine consumption for both marks. Furthermore, ADORA2A (A2AR) was identified as another upstream regulator in the epigenomic data, in striking accordance with the primary ability of caffeine to antagonize adenosine receptors (20). Altogether, these data show that in the bulk hippocampus, chronic caffeine treatment induces an overall deacetylation of two active transcription marks, H3K27ac and H3K9/14ac, on genes related to translation, lipid and glucose/insulin-related metabolisms.

To assess whether this histone acetylation depletion exerts an effect on gene transcription, we performed RNA-sequencing (RNA-seq) of both water and caffeine-treated mice. Although differential expression analysis revealed no statistically significant changes of gene expression between groups **(Supplemental Figure 2A)**, relative quantification of the gene expression (z-score) corresponding to all H3K27ac-depleted loci showed an overall decrease in expression **(Supplemental Figure 2B)** over the same number of randomly chosen genes. Furthermore, we also checked by RT-qPCR (n=5-6/group) expression levels of several genes chosen amongst the most depleted ones in H3K27ac and observed a decreased expression following chronic caffeine treatment **(Supplemental Figure 2D, red columns)**. Importantly, we found that some of these genes, such as PBX Homeobox 1 (*Pbx1)*, NAD Kinase 2 (*Nadk2)* and Spindle And Centriole Associated Protein 1 (*Spice1)*, displayed decreased expression not only upon chronic (2 weeks) but also following an acute (24h) caffeine treatment (**Supplemental Figure 2D,** green columns). However, the Cytochrome P450 Family 51 Subfamily A Member 1 (*Cyp51)* gene, that plays a central role in cholesterol and lipid metabolisms, showed decreased expression solely upon chronic caffeine treatment. Moreover, a persistent effect of caffeine on gene expression was observed for *Pbx1* and *Nadk2* genes, as their expression

remained decreased even after a 2-week caffeine withdrawal following chronic administration **(Supplemental Figure 2D,** blue columns**)**.

Impact of chronic caffeine consumption on hippocampal metabolome. Considering that caffeine decreased histone acetylation of metabolic-related genes, we further assessed the impact of the decreased histone acetylation on the hippocampal metabolome. To do so, tissue spatial distribution of molecules was visualized by MALDI (matrix assisted laser desorption ionization) mass spectrometry imaging analysis, acquired from the dorsal hippocampus (Bregma -1.7mm; **Figure 2A**) of water and caffeine-treated mice (n=6/group). PCA analysis was then performed on the recorded mass spectrometry images from both mouse groups (water and caffeine-treated), in order to highlight differences in their hippocampal molecular distribution profiles **(Figure 2B)**. This revealed lipidomic and metabolomic signatures related to chronic caffeine intake, resulting in two distinctly separated clusters. The identification of metabolites and lipids was based on the measurement of their *m/z* and subsequent comparison with different databanks. In total, 59% of the metabolome was assigned to the biochemical class of metabolites (27%) and lipids (32%) **(Figure 2C)**. The *m/z* value of the remaining 41% did not allow for a univocal assignment to a specific biochemical class. Ultimately, statistical analysis of the molecular datasets revealed that chronic caffeine consumption induced a major decrease in metabolites and lipid levels (92% decreased *vs.* 8% increased; **Figure 2D**). The identified species between water and caffeine groups ($p < 0.05$), detected in positive and negative ionization mode, are listed in **Supplemental Table 5**. Related molecular images taken from hippocampi of water and caffeine-treated mice, showing their different levels and distribution are displayed in **Figure 2E**.

Proteomic hippocampal signature associated with chronic caffeine consumption. To gain insights into the potential effect of chronic caffeine intake at the protein level, we performed mass spectrometry proteomic analysis of the bulk dorsal hippocampus of water (control) and chronic

caffeine-treated mice (n=3/group). Caffeine induced alterations of 179 proteins, of which 49 displayed decreased and 130 increased expression levels **(Figure 3A, Supplemental Table 6)**. In line with the two previous datasets (epigenomics and metabolomics), gene ontology and protein network analysis revealed that decreased proteins were again associated with peptide and cellular amide metabolic processes as well as with mitochondria, with reduction of NADH:Ubiquinone Oxidoreductase Subunit A3 (NDUFA3) involved in mitochondrial respiratory chain complex I assembly, of Mitochondrial Pyruvate Carrier 1 (MPC1) responsible for transporting pyruvate into mitochondria or of Long-Chain-Fatty-Acid-CoA Ligase 4 (ACSL4) involved in lipid metabolism **(Figure 3B)**. Together, these three approaches suggest a robust decrease in metabolic processes induced by chronic caffeine intake in the bulk hippocampal tissue. 35 out of the 49 proteins decreased by caffeine, including Insulin Degrading Enzyme (IDE) and NDUFA3, were reversed by caffeine withdrawal. Only 14 proteins, such as Insulin Like Growth Factor 2 Receptor (IGF2R) remained decreased following caffeine withdrawal **(Supplemental Table 6)**.

Gene Ontology analysis of the increased proteins revealed three main protein clusters: one related with RNA-binding and spliceosome, a second linked to autophagosome and protein processing to endoplasmic reticulum, and a last one associated with glutamatergic synapse and phosphatase activity. Considering that caffeine induced expression of some synaptic proteins, and controls glutamatergic synaptic transmission (e.g. (19), we further assessed their predicted role in the synaptic compartment using the Synaptic Gene Ontologies and annotations (SynGO) (26). We observed that most of the synaptic proteins annotated were related to synaptic organization and signaling, more particularly, to chemical synaptic transmission, such as SH3 And Multiple Ankyrin Repeat Domains 3 (SHANK3) that encodes critical scaffolding proteins for glutamatergic neurotransmission in the post-synaptic densities (27), Synaptopodin (SYNPO) a part of the actin cytoskeleton of postsynaptic densities (28) or CREB–Regulated Transcription Coactivator 1 (CRTC1) involved in hippocampal plasticity and memory (29). Overall, proteomic analysis revealed a decrease in metabolism-related proteins, concomitant with an increase of neuronal/synapse-

associated proteins. Interestingly, 57 out of the 130 proteins increased by chronic caffeine intake, including SHANK3 and synaptopodin (SYNPO) were reversed 2 weeks after caffeine withdrawal, while the other 73 proteins maintained a persistent increase. The latter includes the ATPase Family AAA Domain Containing 1 (ATAD1) protein that controls synaptic plasticity by regulating the release of neurotransmitter receptors from postsynaptic scaffolds (30) **(Supplemental Table 6)**.

Neuronal-specific H3K27ac in synaptic transmission-related genes is increased by chronic caffeine consumption. Our epigenomic data performed in bulk tissue revealed a robust decrease of histone acetylation (H3K27ac and H3K9/14ac) **(Figure 1)**. However, increased synaptic proteins observed following mass spectrometry proteomics in caffeine-treated mice supported a presumable neuron-autonomous impact of caffeine and stressed the importance of conducting cell-type specific experiments to better understand caffeine-induced adaptive alterations of neuronal/synaptic transmission. Thus, to assess cell-specific effects, we analyzed the epigenome of neuronal-enriched populations derived from water and caffeine-treated mouse dorsal hippocampi. We used a novel enzyme-tethering strategy, the Cleavage Under Targets and Tagmentation (CUT&Tag) approach, instead of the ChIP-seq, that allows the profiling of a lower number of cells at higher resolution (31). We first validated the CUT&Tag-seq approach by analyzing H3K27ac signatures in a hippocampal cell suspension (all cells) and compared with ChIP-seq results obtained in bulk tissue. In all cells, CUT&Tag-seq analysis revealed a strong depletion on H3K27ac in caffeine treated-mice as observed by ChIP-seq **(Supplemental Figure 3A)**. IPA analysis of the depleted H3K27ac genes revealed common upstream regulators (TCF7L2, MKNK1, NFASC) with these two different experimental designs **(Supplemental Figure 3B)**. Additionally, a robust overlap was found on the KEGG pathways of the common acetylation depleted genes obtained with CUT&Tag and ChIP-seq analyses **(Supplemental Figure 3C)**. We then proceeded with the neuronal epigenetic study by CUT&Tag-seq using H3K27ac, the latter mark having displayed the stronger caffeine-associated alterations in bulk ChIP-experiments. In addition, we investigated a repressive version of this mark,

the trimethylation of H3 histone lysine 27 (H3K27me3) to strengthen our results with additional information **(Figure 4A)**. We first confirmed that neuronal genes were enriched in H3K27ac and depleted in H3K27me3 in our neuronal enriched cellular fraction, when the opposite was seen on a set of glial-associated genes **(Supplemental Figure 4A).** In sharp contrast with data obtained from bulk hippocampal tissue, differential analyses of caffeine-treated and control mice revealed a preponderance of H3K27ac-enriched regions in neurons obtained from caffeine-treated mice (7127, FDR<10E-6) as compared to the number of depleted regions (4343, FDR<10E-6) **(Figure 4B, Supplemental Table 8)**. H3K27ac PCA plot indicated a separation between the two groups with a PC1 of 58% **(Supplemental Figure 4B)**. While decreased regions were found in genes mostly associated with immune response **(Supplemental Figure 5A)**, increased regions-associated genes were strongly related to the synaptic compartment involved in the regulation of synaptic plasticity, action potential, LTP and memory (see DAVID: GO cellular component and GREAT: GO Biological process) **(Figure 4C).** The repressive mark, H3K27me3, displayed also a higher number of enriched regions (2734, FDR<10E-6) compared with depleted ones (1712, FDR<10E-6) **(Figure 4D; Supplemental Table 8)**. H3K27me3 PCA plot indicated a separation between the two groups with a PC1 of 53% **(Supplemental Figure 4C)**. Strikingly, H3K27me3 depleted regions-associated genes in neurons were mostly linked to ion transport processes, such as calcium and potassium transport, as well as chemical synaptic transmission and learning **(Figure 4E)**, while enriched regions were associated with transcription and histone deacetylase binding-related processes **(Supplemental Figure 5B)**. Analysis of the intersected regions depleted in acetylation and increased in methylation showed 282 regions which corresponding to genes linked to the transcription machinery (**Supplemental Figures 5C,D, blue)**. The opposite overlap showing regions enriched in acetylation and depleted in methylation represented 352 regions that were linked to ion transport functions **(Supplemental Figures 5C,D; red)**. This suggests that pathways linked to synaptic transmission, learning and regulation of membrane potential are co-regulated in neurons by chronic caffeine treatment leading to H3K27 acetylation enrichment and tri-methylation depletion, also clearly

visualized by cluster profiling representation **(Supplemental Figure 5E)**. Finally, integration between neuronal-specific epigenomic data and proteomic data showed that 28 out of the 130 proteins increased by caffeine exhibited a significant H3K27ac enrichment at their coding sequence, mostly related to synapses, particularly to glutamatergic synapses **(Figure 4F)**. These 28 genes/proteins include the calcium binding protein membrane-Associated Phosphatidylinositol Transfer Protein 3 (*Pitpnm3*), as well as the Tetratricopeptide Repeat, Ankyrin Repeat and Coiled-Coil Containing 1 (*Tanc1*), which is a PSD-95-interacting protein regulating dendritic spines at excitatory synapses (32). Among these 28 genes/proteins, we also identified the CREB Regulated Transcription Coactivator 1 (*Crtc1*), required for efficient induction of CREB target genes to engage activity-dependent transcription during neuronal activity (33) **(Figure 4G)**. Overall, these findings suggest that chronic caffeine intake exerts a cell-autonomous positive epigenetic modulation of the synaptic transmission and plasticity processes in hippocampal neurons.

Chronic caffeine consumption enhances learning-dependent hippocampal transcription. We finally aimed at addressing whether chronic caffeine consumption had an impact on transcriptional regulations induced by learning processes. Two experimental conditions were assessed: “Home cage” conditions, consisting of resting mice and “Learning” conditions, consisting of 3 days of training for spatial memory using the Morris Water Maze task, a hippocampal-dependent task (**Figure 5A**). The learning groups showed a better acquisition of the hidden platform position at the third day of training (D3), revealed by the decreased distance traveled during the last day **(Supplemental Figure 6**, left panel). Caffeine-treated animals spent significantly less time in the thigmotaxic zone than the water-treated mice (**Supplemental Figure 6**, middle panel). The mean speed *per* day was similar in both learning groups **(Supplemental Figure 6**, right panel). RNA-sequencing (RNA-seq) experiments were then performed in the dorsal hippocampus in both "Home cage" and "Learning" conditions (3 days of training + 1hr (34)) (**Figure 5B;** n=4/group). Interestingly, when the response to training (Learning *versus* Home cage condition) was evaluated, differences emerged between the

water and caffeine-treated groups. While the expression of 209 genes was significantly modified by learning in the water group (47 down- and 162 up-regulated), the caffeine-treated mice displayed about 5-times more genes with altered expression in response to learning, i.e. 1139 (419 down- and 720 up-regulated) **(Figures 5C,D; Supplemental Table 9)**. In resting mice, while none of the genes were significantly modified by chronic caffeine treatment **(Supplemental Figure 2A)**, z-scores of the group of genes that were significantly down-regulated by learning (419 down) displayed increased basal expression levels and decreased levels upon learning, thus showing a higher amplitude of expression level **(Figure 5E, left panel)**. Likewise, higher amplitude of expression was observed on up-regulated genes by learning (720 up), as they presented decreased expression levels in resting mice and increased expression levels in response to training **(Figure 5E, right panel)**. The 419 down-regulated genes by caffeine plus training were significantly associated with "ribosome" KEGG pathway (**Figure 5F**). Since we previously found that chronic caffeine treatment pointed to the common GO Biological process term: "translation" (ChIP-seq data, **Figure 1B,D**) and the common potential upstream regulator MKNK1 (**Supplemental Table 4 and 7**), these RNA-seq data indicate that chronic caffeine treatment may have a functional effect on the general translation processes already in resting mice, which can be amplified when the system is activated. The same reasoning holds true for genes that are induced upon chronic caffeine and training: genes induced by training in water-treated animals were associated with transcriptional processes (**Figure 5G,** dashed black bars) similarly to the caffeine-treated group (**Figure 5h,** dashed blue bars); however, caffeine treatment increased the significance of transcriptional pathways in response to learning as compared to water-treated mice **(Figure 5G)**. Accordingly, the immediate early gene *Fosb*, as well as the *Xbp1* gene, which is known to play an important role in memory formation (35), were significantly more activated by the learning process under caffeine treatment **(Supplemental Figure 7A)**. Caffeine treatment also promoted the activation of other pathways related to metal ion binding or transferase/ligase/kinase activities (**Figure 5G,** dashed blue bars). Among the 607 genes specifically upregulated in caffeine-treated animals under learning conditions, we identified *Vegfa*, an important

modulator of hippocampal neurogenesis and cognition (36) and *Acss1*, an Acetyl-CoA Synthetase-coding gene, whose related family member *Acss2* regulates histone acetylation and hippocampal-dependent memory (37) **(Supplemental Figure 7B)**. Further integration of the 720 up-regulated genes by learning in caffeine-treated animals revealed that 121 of them were already de-acetylated (H3K27ac ChIP-seq) in resting conditions **(Figure 5H)**, in coherence with their decreased expression (z-score) levels in home-cage caffeine *versus* water **(Figure 5I)**. Strikingly, these genes were strongly related to metabolic processes **(Figure 5J)**, suggesting that caffeine plays a role on re-setting histone acetylation profiles of metabolic genes in bulk tissue (i.e. presumably in non-neuronal cells), so that they become highly inducible by learning conditions (when metabolic support is most required)**.** In support, we further confirmed these findings by integrating these RNA-seq data with the H3K27ac CUT&Tag-seq datasets using all cells **(Supplemental Figure 7C,D,E)**.

Discussion

Caffeine is the most widely consumed psychoactive drug. However, there is a striking mismatch between the epidemiological evidence associating the regular intake of caffeine with benefits for chronic brain disorders and the molecular clarification of the impact of caffeine on brain function. In fact, the majority of molecular and neurophysiological studies explored the impact of acute rather than repeated exposure to caffeine, which have been documented to differently impact on brain function (38–40). Herein, using a combination of different non-hypothesis driven-omic approaches, we show that, in the bulk tissue analysis, chronic caffeine treatment reduced metabolic processes related to lipids, mitochondria and translation in the mouse hippocampus, some of which were identified at the different molecular levels analyzed, *i.e.* epigenome, transcriptome, proteome and metabolome. In sharp contrast to what was observed in bulk tissue, we found that caffeine induced a neuronal autonomous epigenomic response related to synaptic plasticity activation. These data were corroborated by the fact that caffeine treatment induced an increase in glutamatergic synapse proteins in the hippocampus and ultimately, enhanced transcriptomic regulations in response to learning. Overall, our data prompt the novel concept that regular caffeine intake promotes a more efficient ability of the brain to encode experience-related events. By coordinating epigenomic changes in neuronal and non-neuronal cells, regular caffeine intake promotes a fine-tuning of metabolism in resting conditions, likely improving neuronal activity in response to learning.

A major finding of this study is the observation that a 2-weeks exposure to caffeine induced a prominent decrease of histone acetylation (H3K27ac and H3K9/K14ac) in genes associated with several metabolic processes in the dorsal hippocampus in basal/resting conditions. H3K27ac depleted genes had decreased z-score levels in the caffeine-treated group, suggesting a mild impact on gene transcription as well. These data were supported by a metabolomic study indicating a global decrease of metabolites and lipids in the same experimental conditions, as well as by a proteomic analysis suggesting a decrease in energy metabolism with the reduction of several proteins involved

in mitochondrial activity (e.g. NDUFA3 and MPC1). These chronic changes were to some point related to acute caffeine treatment as a few genes were similarly impacted following a 24h and a 2-week caffeine treatment, in line with Yu et al., 2009 (41), but the main changes were associated with long-term exposure to caffeine, as found for e.g. the *Cyp51* gene, encoding a protein involved in cholesterol and lipid metabolism. In accordance, we found that 14 over 49 downregulated hippocampal proteins were still altered despite 2 weeks of caffeine withdrawal, indicating a persistence of chronic caffeine effects, as previously suggested (42). Among these long-lasting impacted proteins by chronic caffeine intake, we found ACSL4 and GNA14, which are involved in the cellular synthesis of fatty acids/lipids, or IGF2 receptor and ITPR3, involved in insulin-dependent regulations. Importantly, these data are in line with and bring molecular support to recent functional magnetic resonance imaging data showing that habitual coffee drinkers exhibit decreased brain functional connectivity at rest (43). As bulk hippocampal tissue was investigated, a question lies in understanding the cellular types underlying such metabolic decrease. Independent IPA analysis of our two sets of epigenomic data (ChIP-seq on bulk hippocampal tissue and CUT&Tag-seq on dissociated hippocampal cells, “all cells”) particularly pointed at three common upstream regulators: TCF7L2 (transcription factor 7 like 2), MKNK1 (MAPK interacting serine/threonine kinase 1) and NFASC (neurofascin). In the mouse brain, these genes are predominantly expressed by non-neuronal cells: TCF7L2 is preferentially expressed by newly formed oligodendrocytes and astrocytes, NFASC in newly formed oligodendrocytes, while MKNK1 is particularly enriched in microglia (see https://www.brainrnaseq.org/). IPA analysis of “all cells” CUT&Tag-seq data further highlighted the involvement of GLI1 and SOX2, that are both particularly enriched in astrocytes. These observations strongly support that the basal/resting signatures elicited by chronic caffeine intake may rely on non-neuronal, likely glial, responses.

Concomitant with this de-acetylation process observed in the bulk hippocampus, we showed that chronic caffeine was able to induce a neuron-autonomous epigenomic response using both active (H3K27ac) and repressive (H3K27me3) marks: acetylation of H3K27 was enriched while its tri-

methylation was depleted at genes related to membrane potential, potassium ion regulation and learning and memory processes. This suggests that the overall chronic caffeine effect positively regulates neuronal activity and synaptic transmission. Proteomic studies supported this argument as a series of identified upregulated proteins were related to the glutamatergic synapse. It is interesting to note that 73 out of 130 upregulated proteins -some of them related to the synapse- remained elevated even after a 2-weeks caffeine withdrawal, revealing a long-lasting impact of chronic caffeine intake on neurons. Integration of epigenomic and proteomic data particularly pointed towards CRTC1, known to act as a coincidence sensor of calcium and cAMP signals in neurons triggering a transcriptional response involved in late-phase LTP maintenance at hippocampal synapses (44). We further observed that chronic caffeine intake impacts the learning/training-induced transcriptome by significantly enhancing the number of differentially regulated genes. Integration of the learning-induced genes with epigenomic data identified a group of 121 genes related to metabolic processes that, besides being over-activated in caffeine-treated mice in learning conditions, were also de-acetylated with decreased overall expression in resting conditions (z-score). This suggests that the resting-state effect of caffeine in non-neuronal/glial cells might be a pre-requisite to the robust activation of metabolic pathways then improving quality and precision of learning-associated processes, in line with its cognitive enhancing function.

Thus, a major overall conclusion of the present study is the ability of regular caffeine intake to exert a long-term effect on neuronal activity/plasticity in the adult brain, through concerted actions on the epigenome, transcriptome, proteome and metabolome, ultimately lowering metabolic-related processes; and to simultaneously finely tuning activity-dependent regulations for a more efficient response to experience. In other words, in non-neuronal cells caffeine decreases -omic activities under basal conditions and improves the signal-to-noise ratio during information encoding in brain circuits, thus contributing to bolster the salience of information in brain circuits. Remarkably, this dual and opposite impact of caffeine under resting conditions and upon brain activation is in line with human brain imaging studies: under basal conditions caffeine increased brain entropy (45) and

decreased functional connectivity (46), whereas it increases BOLD activation in the frontopolar and cingulate cortex in a verbal working memory task (47) reflecting an increased processing potential. Additionally, neurophysiological studies on the putative targets of caffeine - adenosine receptors – are in line with this dual role of caffeine, as shown by the opposite effects of $A_{2A}R$ to enhance glutamate release contrasting with the A_1R-mediated inhibition of basal synaptic transmission (48), which is also controlled by $A_{2A}R$ (49). Finally, our data also show that the amplitude of the transcriptomic effects of caffeine was far greater when neuronal networks were activated during the learning process rather than in basal conditions, as noted by others when studying the impact of caffeine on gene expression in the basal ganglia (50). This might particularly relate to a “priming” of neuronal activity which would favor the rise of activity-dependent response, as it has been suggested for the mechanism of action of HDAC inhibitors (51). How caffeine coordinates these epigenomic responses in the different cell types is an interesting question that we are currently pursuing.

Finally, the present study highlights the molecular impact of caffeine in the homeostatic brain, that will deserve further investigations, namely regarding the differential mechanisms operating at the cell-specific level to modulate physiological brain activity in resting and activity settings. Our data have additional far-reaching implications. While it is recognized that caffeine exhibits normalizing properties in models of synaptic dysfunction, as in Alzheimer’s disease (52–54), the cell-specific molecular mechanisms remains to be uncovered. In the opposite side of the allostatic brain spectrum (55), caffeine has been suggested to impact synaptic fate in brain development (56, 57) but the involvement of neuronal *vs*. non-neuronal mechanisms remains ill-defined. It is therefore particularly relevant and important to address, at a larger scale, the integrated actions of caffeine in neuronal *vs*. non-neuronal cells in the immature, homeostatic and ageing brain.

Materials and Methods

Animals. Male C57Bl6/J mice (Charles River Laboratories, France) were housed in a pathogen-free facility (University of Lille, France). Mice were 5-6 per cage (GM500, Tecniplast) and maintained under controlled housing conditions for temperature (22°C) and light (12-hour light/dark cycle), with *ad libitum* access to food and water.

Caffeine treatment. Two-three-months-old mice were randomly assigned to the two following experimental groups: water (control) and caffeine. Caffeine solutions were kept in dark bottles thus protected from light and changed weekly. Treatment started at 8-9 weeks of age and lasted for two weeks. The chronic caffeine treatment in mice has been set in order to mimic the usual dose range of caffeine consumption in Humans. The selected caffeine dose of 0.3 g/L p.o., administered through drinking water at 0.3 g/L, has been previously shown to provide a significant benefit in neurodegenerative contexts (54, 58, 59). Regarding the comparison of caffeine exposure for 2 weeks *vs*. 24 hours *vs*. caffeine removal, we proceed as follows: 6 animals were kept under water and other 6 animals were treated with caffeine for 2 weeks and returned to water for 2 additional weeks (caffeine withdrawal group). When the later group of animals returned to water, an additional group that was under water for 2 weeks was then treated with caffeine. A last group was kept under water for 2 weeks and treated with caffeine for only 24 hours. All animals were then sacrificed the same day, the dorsal hippocampus was sampled and stored as indicated below and used for proteomics and RT-qPCR analysis.

Quantitative determination of caffeine and metabolites in brain samples. Brain tissues from water and caffeine groups were used to assess concentrations of caffeine and its metabolites (paraxanthine, theobromine and theophylline). Samples were weighed and 1 mL of 1% formic acid (FA) solution was added to each sample. To determine the recovery rate, control samples were

spiked with a mixture of caffeine, paraxanthine, theobromine and theophylline (10 µM each). The tissues were lysed using 7 mm stainless steel beads and Tissue Lyser LT (Qiagen) for 8 min at 50 strokes/minute, then treated with an ultrasonic bath for 5 minutes and subsequently centrifuged for 15 minutes at 23000x*g* and 4°C. The supernatants were transferred to Amicon® Ultra 2 ml 3K centrifugal filter units (Merck). The remaining pellets were subjected to the same protocol of tissue disruption and centrifugation using 1 mL of acidified water (FA 1%). Amicon® filters containing the combined supernatants from the two-fold extraction process were centrifuged for 140 minutes at 7500x*g* and 23°C. Filtrates were used for liquid chromatography-mass spectrometry analysis. Samples were separated by using a Dionex UltiMate 3000 HPLC system with an integrated variable wavelength detector, set at 280 nm, and equipped with a C18 column (EC Nucleodur® C18 Gravity column, 2 mm ID x 50 mm, 3 µm, Macherey & Nagel). Samples (5 µL) were injected at flow rate of 300 µL/minutes. A solvent gradient was run from 90% A (water containing 0.2% FA and 2 mM ammonium acetate) and 10% B (methanol containing 2 mM ammonium acetate) to 50% A and 50% B over 10 minutes.

The eluate was analyzed with a coupled mass spectrometer ESI-micrOTOF-Q (Bruker Daltonics). Data were acquired in positive full scan MS mode with a scan range *m/z* 50-1000. Identification and quantification of the xanthine derivatives were performed using Data Analysis software (Bruker Daltonics). The limit of detection was 5 nM for caffeine and 10 nM for its metabolites (paraxanthine, theobromine and theophylline).

Learning activation in the Morris water maze. An Atlantis Morris Water Maze (MWM) tank was placed in a room with several visual extra-maze cues. Water opacified with powdered chalk (*Blanc de meudon*) was maintained at a temperature of 21°C. Mice from water (control) and caffeine groups were habituated to the set-up for two consecutive days (habituation 1 and 2). During habituation 1, mice were allowed to discover the pool filled with 5 cm height of water and a visible platform during 60 seconds. During habituation 2, mice were allowed to swim in the pool filled with water in absence

of the platform for 60 seconds. The following 3 days (acquisition day 1–3), mice were trained to localize the platform hidden underneath the opacified water using the spatial cues present in the room. In each acquisition day, mice performed four trials each of 60 seconds maximal duration. Each trial was terminated when the mouse reached the platform or after the 60 seconds. Mice failing to find the platform were gently guided to the platform and allowed to stay for 8–10 seconds. During the training days, mice were subjected to MWM in a random order, so that they were tested at different times of the day. All MWM evaluations of caffeine- or water-treated mice were performed by experimenter blind to mouse treatments.

Sacrifice and brain tissue preparation. For transcriptomic analysis, mice from Learning group were killed by cervical dislocation, one hour after the last training section, while mice from the Home cage group were killed at the same time. Freshly dissected tissues were immediately frozen in liquid nitrogen and kept at -80°C until RNA extraction. Similar sacrifice procedures were used for animals used for proteomic and RTqPCR analyses. For molecular MALDI imaging experiments, mice were deeply anesthetized with sodium pentobarbital (50 mg/kg, *i.p.*), and then transcardially perfused with cold NaCl (0.9%). Brains were collected, frozen on dry ice and stored at -80°C until use.

RNA-seq analysis. Total RNA was extracted from dorsal hippocampal tissues using TRIzol reagent (Invitrogen) (n=4/group). Freshly dissected tissue was chopped, homogenized in 300 µL of TRIzol reagent, and frozen (20 minutes at -80°C), followed by 3-minutes centrifugation at 14000x*g* before chloroform/isoamyl extraction. The supernatant was used to precipitate RNA with isopropanol and RNase-free glycogen (30 minutes at 4°C). The pellet was washed once with 70% ethanol and resuspended in Milli-Q water. A new RNA precipitation was performed with 100% ethanol and 3 M sodium acetate (overnight at -20°C). After two further 70% ethanol washes, the pellet was air-dried and resuspended in 30 µL nuclease-free Milli-Q water, heated 6 minutes at 50°C, and RNA quantification was performed. RNA-seq libraries (n=4/group) were generated from 500 ng of total

RNA using Illumina® TruSeq® Stranded mRNA Library Prep Kit v2. Briefly, following purification with poly-T oligo attached magnetic beads, the mRNA was fragmented using divalent cations at 94°C for 2 minutes. The cleaved RNA fragments were copied into first-strand cDNA using reverse transcriptase and random primers. Strand specificity was achieved by replacing dTTP with dUTP during the second-strand cDNA synthesis by DNA Polymerase I and RNase H. Following the addition of a single "A" base and the subsequent ligation of the adapter on double-stranded cDNA fragments, the products were purified and enriched with PCR [30 s at 98°C; (10 seconds at 98°C, 30 seconds at 60°C, 30 seconds at 72°C) × 12 cycles; 5 minutes at 72°C] to create the cDNA library. Surplus PCR primers were further removed by purification using AMPure XP beads (Beckman Coulter), and the final cDNA libraries were checked for quality and quantified using capillary electrophoresis. Sequencing was performed on the Illumina® Genome Hiseq4000 as single-end 50 base reads following Illumina's instructions. Reads were mapped onto the mm10 assembly of *Mus musculus* genome using STAR v2.5.3a (60) and the Bowtie 2 aligner v2.2.8 (61). Only uniquely aligned reads were kept for further analyses. Quantification of gene expression was performed using HTSeq-count v0.6.1p1 (62) and gene annotations from Ensembl release 90 and "union" mode. Read counts were normalized across libraries with the method proposed by Ander et al. (2010) (63). Comparisons of interest were performed using the test for differential expression proposed by Love (64) and implemented in the DESeq2 Bioconductor library (v1.16.1). Resulting p-values were adjusted for multiple testing using the Benjamini and Hochberg method (65).

Chromatin Immunoprecipitation (ChIP). Freshly dissected tissue was chopped by a razor blade and rapidly incubated in 1.5 mL phosphate-buffered saline (PBS) containing 1% formaldehyde for 10 minutes at room temperature. To stop fixation, glycine was added (0.125 M final concentration). Dorsal hippocampi from 4 mice were pooled per sample and two biological replicates *per* condition were used for the ChIP-seq. Tissue samples were then processed as described in Chatterjee *et al.* (34) and sonicated using the Diagenode Bioruptor (30 seconds ON-30 seconds OFF at High Power

x 35 cycles). Sonicated chromatin was centrifuged 10 minutes at 14000x*g*, the supernatant collected and diluted 1:10 in ChIP dilution buffer (0.01% SDS, 1.1% Triton X-100, 1.2 mM EDTA, 16.7 mM Tris-Cl, pH 8.1, 167 mM NaCl). A fraction of the supernatant (50 μL – 10%) from each sample was saved before immune-precipitation for 'total input chromatin'. Supernatants were incubated overnight (4°C) with 1/1000 primary antibodies against H3K9/14ac (Diagenode #C15410200) and H3K27ac (Abcam #ab4729), followed by protein A Dynabeads (Invitrogen) for 2 hours at room temperature. After several washes (low salt, high salt, LiCl and TE buffers), the resulting DNA-protein complexes were eluted in 300 μL elution buffer (1% SDS, 0.1 M $NaHCO_3$). The crosslinking was reversed (overnight at 65°C) and the DNA was subsequently purified with RNAse (30 minutes at 37°C) and proteinase K (2 hours at 45°C). DNA from the immunoprecipitated and input samples was isolated using Diagenode MicroChIP DiaPure columns with 20 μL nuclease-free milliQ water in low binding tubes. ChIP samples were further purified at the Genomeast Platform using Agencourt AMPure XP beads (Beckman Coulter) and quantified using Qubit (Invitrogen).

ChIP-seq libraries and sequencing. ChIP-seq libraries were prepared from 2-10 ng of double-stranded purified DNA using the MicroPlex Library Preparation kit v2 (C05010014, Diagenode s.a., Seraing, Belgium), according to manufacturer's instructions. DNA was first repaired and yielded molecules with blunt ends. Next, stem-loop adaptors with blocked 5' ends were ligated to the 5' end of the genomic DNA (gDNA), leaving a nick at the 3' end. The adaptors cannot ligate to each other and do not have single-strand tails thus non-specific background is avoided. In the final step, the 3' ends of the gDNA were extended to complete library synthesis and Illumina compatible indexes were added through a PCR amplification (4+7 cycles). Amplified libraries were purified and size-selected using Agencourt AMPure XP beads (Beckman Coulter) to remove unincorporated primers and other reagents. Prior to analyses, DNA libraries were checked for quality and quantified using a 2100 Bioanalyzer (Agilent). The libraries were loaded in the flowcell at 8 pM concentration, and clusters

were generated using the Cbot and sequenced using the Illumina HiSeq 4000 technology as single-end 50 base reads following Illumina's instructions. Image analysis and base calling were performed using RTA and CASAVA.

ChIP-seq analyses. Sequenced reads were mapped to the *Mus musculus* genome assembly mm10 using Bowtie v1.0.0 with the following parameters «-m1-strata-best-y-l40». Samtools merge v1.3.1 (66) was used to combine biological replicates by condition. Then, BEDtools intersect v2.26.0 (67) was used to remove reads located within ENCODE blacklisted regions. SICER (SICER-df.sh) v1.1 (68) was used to detect differentially bound regions on the pools of biological replicates using the following parameters: «Species: mm10, Effective genome size as a fraction of reference genome: 0.74, Threshold for redundancy allowed for treated reads: 1, Threshold for redundancy allowed for WT reads: 1, Window size: 200 bps, Fragment size: 200 bps, Gap size: 600 bps, FDR for identification of enriched islands: 1E-2, FDR for identification of significant changes: 1E-2. Finally, differentially bound regions were annotated with respect to the closest gene using Homer annotatePeaks.pl v4.11.1 (69). An FDR of 1E-5 was used in differential analyses (caffeine *vs*. control).

Neuronal and all cells isolation. Neuronal and all cells suspensions were obtained from mouse hippocampus chronically treated with caffeine or water (control). For that, we used Neural Tissue Dissociation (Miltenyi, #130-092-628) and Neuron Isolation Kits (Miltenyi, #130-115-389), following manufacturer's instructions with some adaptations. Briefly, two mouse hippocampi were pooled *per* sample and harvested in a pre-heated buffer solution containing papain. This was followed by series of manual mechanical dissociations, using scissors and fire polished Pasteur pipettes of descending diameter, and incubations at 37°C under slow rotation. The solution was then filtered (50 µm) and centrifuged (10 minutes, 300x*g*, at room temperature) and myelin was removed using Myelin Removal Beads II kit (Miltenyi, #130-096-733), incubating for 15 minutes at 4°C, centrifuging (10

minutes, 300x*g* at 4°C) and filtering the sample through MS columns (Miltenyi, #130-042-201) placed in MiniMACS™ Separator (Miltenyi, #130-042-102) to collect the myelin depleted flow-through, free of cell debris. The 'all cells' suspension was collected at this point and counted using the TC20 Automated Cell Counter (Bio-Rad, #1450102) to obtain a total of 70,000 cells *per* sample. With the remaining of the samples, we proceeded with neuronal isolation according to manufacturer's instructions, finally depleting the samples through MS columns to collect the flow-through enriched in neurons. The samples were counted and 70,000 cells *per* sample were taken for CUT&Tag experiments.

Cleavage Under Targets and Tagmentation (CUT&Tag). Having isolated all cells and neuronal populations we proceeded with CUT&Tag method to assess their genome-wide H3K27ac and H3K27me3 chromatin state. The protocol was adapted from that described by Kaya-Okur *et al.*, 2019 (31) The method is based on digitonin-induced cell permeabilization (Sigma, #300410-250MG) and concanavalin A-coated magnetic beads (Cell signaling, #93569S) immobilization. This is followed by over-night incubation at 4°C with primary antibodies against H3K27ac (Abcam, #ab4729) and H3K27me3 (Diagenode, #C15410195), followed by 1 hour incubation with the secondary antibody (Antibodies online, #ABIN101961). The loaded-Tn5 is then added (Diagenode, #C01070001) and the cleaved DNA is extracted using MinElute PCR Purification Kit (Quiagen, # 28004). Library preparation was conducted using Nextera primers (Illumina, #FC-131-2001) and post-PCR clean-up using SPRI bead slurry (Beckmann Coulter, #B23317). Concentration of the collected DNA was achieved by Qubit (Invitrogen, #Q32851). Two biological replicates were used *per* group and Rabbit IgG (Diagenode #C15410206) was used as control.

CUT&Tag analyses. Reads (paired-end) were mapped to *Mus musculus* genome (assembly mm10) using Bowtie2 (61) v2.2.8 with default parameters except for "–end-to-end-very-sensitive-no-mixed –no-discordant-I10-X700". Prior to peak calling, reads with mapping quality below 30 were removed

using samtools v1.13 (66) with the command line “samtools view-b-q30.” Then, reads falling into Encode blacklisted regions v2 (70) were removed using BEDtools intersect v2.30.0 (67). Biological replicates were pooled (n=2) using samtools merge v1.13 (66). Then, peak calling was done with SICER v1.1 (69) with the following parameters: Window size: 200 bps; Gap size: 800 (H3K27ac) and 1200 (H3K27me3). Detected peaks were combined to get the union of all peaks using the tool Bedtools merge v2.30.0 (67). Differentially bound regions were detected used SICER v1.1 and annotated relative to genomic features using Homer v4.11.1 (71). An FDR<1E-5 was used for further analyses (caffeine *vs*. control) in all cells and neuronal enriched population.

Mass spectrometry proteomic analysis. 100 µg of proteins were digested from dorsal hippocampus (n=3/group) with trypsin by FASP method. Peptides were fractionated with 4 increments (7.5, 12.5, 17.5 and 50%) of acetonitrile in 0.1% TEA on High pH Reversed-Phase - Peptide Fractionation Kit (Thermo Fisher Scientific). Eluents were dried by vacuum centrifugation and resolved in 0.1% formic acid. An UltiMate 3000 RSLCnano System (Thermo Fisher Scientific) was used for separation of the eluents. Peptides were automatically fractionated onto a commercial C18 reversed phase column (75 µm × 500 mm, 2-µm particle, PepMap100 RSLC column, Thermo Fisher Scientific, temperature 55 °C). Trapping was performed during 4 minutes at 5 µL/minute, with solvent A (98% H_2O, 2% acetonitrile and 0.1% formic acid). The peptides were eluted using two solvents A (0.1% formic acid in water) and B (0.1% formic acid in acetonitrile) at a flow rate of 300 nL/minute. Gradient separation was 3 minutes at 3% B, 170 minutes from 3 to 20% B, 20 minutes from 20% B to 80% B and maintained for 15 minutes at 80% B. The column was equilibrated for 17 minutes with 3% buffer B prior to the next sample analysis. The eluted peptides from the C18 column were analyzed by Q-Exactive instruments (Thermo Fisher Scientific). The electrospray voltage was 1.9 kV, and the capillary temperature was 275 °C. Full MS scans were acquired in the Orbitrap mass analyzer over *m*/*z* 400–1200 range with a 70,000 (*m*/*z* 200) resolution. The target value was 3.00E+06. The fifteen most intense peaks with charge state between 2 and 5 were fragmented in

the higher-energy collision-activated dissociation cell with normalized collision energy of 27%, and tandem mass spectrum was acquired in the Orbitrap mass analyzer with a 17,500 (*m*/*z* 200) resolution. The target value was 1.00E+05. The ion selection threshold was 5.0E+04 counts, and the maximum allowed ion accumulation times were 250 ms for full MS scans and 100 ms for tandem mass spectrum. Dynamic exclusion was set to 30 s.

Proteomic data analysis. Raw data collected during nanoLC–MS/MS analyses were processed and converted into a *.mgf peak list format with Proteome Discoverer 1.4 (Thermo Fisher Scientific). MS/MS data were analyzed using search engine Mascot (version 2.4.0, Matrix Science, London, UK) installed on a local server. Searches were performed with a tolerance on mass measurement of 10 ppm for precursor and 0.02 Da for fragment ions, against a composite target-decoy database (17125*2 total entries) built with a *Mus musculus* Swissprot database (taxonomy 10090, november 2019, 17007 entries) fused with the sequences of recombinant trypsin and a list of classical contaminants (118 entries). Cysteine carbamidomethylation, methionine oxidation, protein N-terminal acetylation, and cysteine propionamidation were searched as variable modifications. Up to one missed trypsin cleavage was allowed. For each sample, peptides were filtered out according to the cut-off set for protein hits with one or more peptides taller than 9 residues, and a 1% false positive rate.

MALDI mass spectrometry imaging (MSI) of lipids and metabolites. Hippocampal sections (10 µm) were collected from Bregma -1.7 mm using a CM3050 cryostat (Leica Microsystems; n=6 *per* experimental group) and then mounted on indium tin oxide (ITO)-coated slides for MALDI-MSI and on SuperFrost™ (Thermo Scientific) slides for histological analysis. In order to monitor analytical reproducibility, biological replicates were used for each group. For MALDI-MSI, 1,5-diaminonaphtalene (1,5-DAN) matrix at 10 mg/mL in acetonitrile:H_2O (1:1, v/v) was used in negative ion mode, whereas 2,5-dihydroxybenzoic acid (2,5-DHB) matrix at 40 mg/mL in methanol:H_2O with

0.1% trifluoroacetate (1:1, v/v) was used in positive ion mode. A uniform layer of matrix was deposited on brain tissue sections using an HTX TM-sprayer™ device (HTX Technologies, LLC). Lipids and metabolites imaging was performed on a Solarix 7T MALDI-FTICR instrument (Bruker Daltonics) equipped with a SmartBeamII™ laser and controlled using FtmsFlexControl 2.1.0 software (Bruker Daltonics). Data sets were recorded in full scan negative or positive ion mode using an online calibration from *m/z* 100 to 1000, at a spatial resolution of 35 µm for the hippocampus. MSI data were acquired from each tissue section as well as matrix adjacent control areas in order to check for analyte delocalization eventually occurring during sample preparation. All data processing, visualization and quantification were performed using Multimaging 1.1.9 software (ImaBiotech SAS). For statistical analysis, SCiLS Lab 2015 software (SciLS) was used to perform principal component analysis (PCA) with a Student *t*-test assumed as significant for p-value < 0.05. These analyses were done for both positive and negative ion mode and the significant results were grouped together. Annotation of the discriminant *m/z* was done based on experimental accurate (*m/z*) mass and by using METLIN library (http://metlin.scripp.edu/) and Human Metabolome Database (HMDB) (http://www.hmdb.ca/) with 10 ppm delta error. These online databases are linked to KEGG (http://www.genome.jp/kegg/), PubChem (https://pubchem.ncbi.nlm.nih.gov/) and LIPID MAPS (http://www.lipidmaps.org/), which were used for further investigations. After MSI data acquisition, any residual matrix on the tissue sections was removed with a 100% methanol washing. Tissue sections were then stained with Nissl dye and high-definition histological images were acquired using a Pannoramic digital slide scanner (3DHistech Ltd) and then loaded in Multimaging software to perform the high-definition overlays with convoluted molecular images, improving molecular images resolution.

RNA extraction and quantitative real-time PCR analysis (RT-qPCR). Total RNA was extracted from dorsal hippocampi and purified using the RNeasy Lipid Tissue Mini Kit (Qiagen, France). 500 ng of total RNA were reverse-transcribed using the Applied Biosystems High-Capacity cDNA reverse

transcription kit. Real time PCR was performed on a StepOne device using Taqman Gene Expression Master Mix (Thermo Fisher), following manufacturer's recommendations. Expression levels of the following genes were evaluated by the comparative CT method (2- deltaCT) using the following Taqman probes: *Cyp51* ID :Mm00490968_m1, *Spice1* ID:Mm00519954_m1, *Nadk2* ID: Mm01297768_m1, *Pbx1* ID: Mm04207617_m1, *Ppia* ID: Mm02342430.

Pathway analysis of epigenomic data. ChIP-seq and CUT&Tag data from hippocampus of water and caffeine-treated mice were uploaded to Ingenuity Pathway Analysis (IPA) software (Qiagen). A p-value < 0.05 with Student's t-test was set as threshold and an integrated pathway analysis of ChIP-seq, proteomic and metabolomic data was performed using the core analysis function, including canonical pathways, upstream regulators, diseases, biological functions and molecular networks filtered by "Central Nervous System"-associated terms.

Statistical Analysis. This omics study includes different statistical approaches that are detailed in the appropriate method paragraph. All data needed to evaluate the conclusions are provided in the paper or the Supplementary Materials. Sequencing data that support the findings of this study have been deposited in GEO with the primary accession code GSE167123. The number of biologically independent experiments, sample size, p values, and statistical tests are all indicated in the main text and/or figure legends. The significance level was set at $p < 0.05$, unless otherwise stated in the figure legend.

Study approval. All experimental protocols were approved by the local Animal Ethical Committee (Agreement #12787-2015101320441671v9 from CEEA75, Lille, France). All procedures complied with European standards for the care and use of laboratory animals.

Author contributions.

Conceptualization: IP, LC, CM, LP, LB, VBS, RAB, NS, JSA, ALB, DB

Methodology: IP, LC, CM, LP, AP, HD, SLG, CEM, EF, KC, SE, JS, JS, ON, JMS, ASL

Investigation: IP, LC, CM, LP, AP, HD, SLG, MS, EMM, EF, KC, VGM, BT, SE, ES, JS, RAB, NS, LT; IG

Data analysis: IP, LC, CM, LP, HD, SLG, CEM, DV, JS, RAB, NS, JSA, ALB, DB, ON, JMS

Supervision: RAB, NS, JSA, ALB, DB

Writing—original draft: LC, IP, CM, LP, DV, LVL, RAC, RAB, NS, JSA, ALB, DB

Writing—review & editing: LC, IP, CM, CEM, TL, LVL, LB, VBS, RAC, NS, JSA, ALB, DB

Acknowledgements. We thank the Animal Facilities (F-59000 Lille, France; F-67000 Strasbourg, France) and Mélanie Besegher, Cyrille Degraeve, Caroline Declerck, Kim Letten, Didier Montignies, Christian Meunier, Laure Taquet and Romain Dehayn (U1172), as well as Olivier Bildstein, Onwukanjo-Daniel Egesi and George Edomwonyi (UMR 7364) for animal care. Sequencing was performed by the GenomEast Platform, a member of the 'France Génomique' consortium (ANR-10-INBS-0009). This work was supported by grants from Hauts-de-France (PARTEN-AIRR, COGNADORA; START-AIRR, INS-SPECT) and Programs d'Investissements d'Avenir LabEx (excellence laboratory) DISTALZ (Development of Innovative Strategies for a Transdisciplinary approach to ALZheimer's disease) and EGID (European Genomic Institute for Diabetes ANR-10-LABX-46). Our laboratories are also supported by ANR (GRAND to LB, ADORATAU, ADORASTrAU, METABOTAU to DB and BETAPLASTICITY to JSA), COEN (5008), Fondation pour la Recherche Médicale, France Alzheimer/Fondation de France, FHU VasCog research network (Lille, France), Fondation Vaincre Alzheimer (ADOMEMOTAU), European Foundation for the Study of Diabetes (EFSD to JSA), Fondation Plan Alzheimer as well as Inserm, CNRS, Université Lille, Lille Métropole Communauté Urbaine, DN2M. KC hold a doctoral grant from Lille University. VG-M was supported by Fondation pour la Recherche Médicale (SPF20160936000). CM was supported by Région Hauts-

de-France. ALB is supported by CNRS, Unistra (Strasbourg, France), ANR-16-CE92-0031 (EPIFUS), ANR-18-CE16-0008-02 (ADORASTrAU), Alsace Alzheimer 67, France Alzheimer (AAP SM 2017 #1664). IP is supported by Fondation pour la Recherche Médicale (SPF201909009162). CEM is grateful for the support by the Alzheimer Forschung Initiative e.V. (AFI, Düsseldorf, Germany). LC was funded by SIF Italian Society of Pharmacology. RAC was supported by LaCaixa Foundation (LCF/PR/HP17/52190001) and FCT (POCI-01-0145-FEDER-03127). Santa Casa da Misericórdia (MB-7-2018) and CEECIND/01497/2017 to LVL.

References

1. Smith A. Effects of caffeine on human behavior.. *Food Chem Toxicol.* 2002;40(9):1243–1255.
2. Kim Y, Je Y, Giovannucci E. Coffee consumption and all-cause and cause-specific mortality: a meta-analysis by potential modifiers.. *Eur J Epidemiol.* 2019;34(8):731–752.
3. Loftfield E et al. Association of Coffee Drinking With Mortality by Genetic Variation in Caffeine Metabolism: Findings From the UK Biobank. *JAMA Intern Med.* 2018;178(8):1086–1097.
4. Freedman ND, Park Y, Abnet CC, Hollenbeck AR, Sinha R. Association of coffee drinking with total and cause-specific mortality. *N Engl J Med.* 2012;366(20):1891–1904.
5. Flaten V et al. From epidemiology to pathophysiology: what about caffeine in Alzheimer's disease? *Biochem Soc Trans.* 2014;42(2):587–592.
6. Cunha RA. How does adenosine control neuronal dysfunction and neurodegeneration?. *J Neurochem.* 2016;139(6):1019–1055.
7. Cellai L et al. The Adenosinergic Signaling: A Complex but Promising Therapeutic Target for Alzheimer's Disease. *Front Neurosci.* 2018;12:520.
8. Wright GA et al. Caffeine in Floral Nectar Enhances a Pollinator's Memory of Reward. *Science.* 2013;339(6124):1202– 1204.
9. Marques S, Batalha VL, Lopes LV, Outeiro TF. Modulating Alzheimer's disease through caffeine: a putative link to epigenetics.. *J Alzheimers Dis.* 2011;24 Suppl 2:161–171.
10. Angelucci MEM, Cesário C, Hiroi RH, Rosalen PL, Da Cunha C. Effects of caffeine on learning and memory in rats tested in the Morris water maze. *Brazilian J Med Biol Res.* 2002;35(10):1201–1208.
11. Borota D et al. Post-study caffeine administration enhances memory consolidation in humans. *Nat Neurosci.* 2014;17(2):201–203.
12. Lopes JP, Pliássova A, Cunha RA. The physiological effects of caffeine on synaptic transmission and plasticity in the mouse hippocampus selectively depend on adenosine A(1) and A(2A) receptors. *Biochem Pharmacol.* 2019;166:313–321.
13. Costenla AR, Cunha RA, de Mendonça A. Caffeine, adenosine receptors, and synaptic plasticity. *J Alzheimers Dis.* 2010;20 Suppl 1:S25-34.
14. Simons SB, Caruana DA, Zhao M, Dudek SM. Caffeine-induced synaptic potentiation in hippocampal CA2 neurons. *Nat Neurosci.* 2011;15(1):23–25.
15. Lao-Peregrín C et al. Caffeine-mediated BDNF release regulates long-term synaptic plasticity through activation of IRS2 signaling. *Addict Biol.* 2017;22(6):1706–1718.

16. Blaise JH, Park JE, Bellas NJ, Gitchell TM, Phan V. Caffeine consumption disrupts hippocampal long-term potentiation in freely behaving rats. *Physiol Rep.* 2018;6(5):e13632.
17. Watanabe Y, Ikegaya Y. Caffeine Increases Hippocampal Sharp Waves in Vitro. *Biol Pharm Bull.* 2017;40(7):1111–1115.
18. Hanajima R et al. Effect of caffeine on long-term potentiation-like effects induced by quadripulse transcranial magnetic stimulation. *Exp Brain Res.* 2019;237(3):647–651.
19. Kerkhofs A et al. Caffeine Controls Glutamatergic Synaptic Transmission and Pyramidal Neuron Excitability in Human Neocortex. *Front Pharmacol.* 2017;8:899.
20. Fredholm BB, Bättig K, Holmén J, Nehlig A, Zvartau EE. Actions of caffeine in the brain with special reference to factors that contribute to its widespread use. *Pharmacol Rev.* 1999;51(1):83–133.
21. Heintzman ND et al. Distinct and predictive chromatin signatures of transcriptional promoters and enhancers in the human genome. *Nat Genet.* 2007;39(3):311–318.
22. Hnisz D et al. Super-enhancers in the control of cell identity and disease. *Cell* 2013;155(4):934–947.
23. J. PSC et al. Chromatin stretch enhancer states drive cell-specific gene regulation and harbor human disease risk variants. *Proc Natl Acad Sci.* 2013;110(44):17921–17926.
24. Karmodiya K, Krebs AR, Oulad-Abdelghani M, Kimura H, Tora L. H3K9 and H3K14 acetylation co-occur at many gene regulatory elements, while H3K14ac marks a subset of inactive inducible promoters in mouse embryonic stem cells. *BMC Genomics* 2012;13:424.
25. Sánchez-Sarasúa S et al. IRS1 expression in hippocampus is age-dependent and is required for mature spine maintenance and neuritogenesis. *Mol Cell Neurosci.* 2022;118:103693.
26. Koopmans F et al. SynGO: An Evidence-Based, Expert-Curated Knowledge Base for the Synapse. *Neuron* 2019;103(2):217-234.e4.
27. Sheng M, Kim E. The Shank family of scaffold proteins. *J Cell Sci.* 2000;113(11):1851–1856.
28. Mundel P et al. Synaptopodin: an actin-associated protein in telencephalic dendrites and renal podocytes. *J Cell Biol.* 1997;139(1):193–204.
29. Parra-Damas A et al. CRTC1 Function During Memory Encoding Is Disrupted in Neurodegeneration. *Biol Psychiatry* 2017;81(2):111–123.
30. Wang L, Walter P. Msp1/ATAD1 in Protein Quality Control and Regulation of Synaptic Activities. *Annu. Rev. Cell Dev Biol.* 2020;36(1):141–164.
31. Kaya-Okur HS et al. CUT&Tag for efficient epigenomic profiling of small samples and single cells. *Nat Commun.* 2019;10(1):1930.
32. Han S et al. Regulation of dendritic spines, spatial memory, and embryonic development by the

TANC family of PSD-95-interacting proteins. *J Neurosci.* 2010;30(45):15102–15112.
33. Parra-Damas A, Rubió-Ferrarons L, Shen J, Saura CA. CRTC1 mediates preferential transcription at neuronal activity-regulated CRE/TATA promoters. *Sci Rep.* 2017;7(1):18004.
34. Chatterjee S et al. Reinstating plasticity and memory in a tauopathy mouse model with an acetyltransferase activator. *EMBO Mol Med.* 2018;10(11).
35. Martínez G et al. Regulation of Memory Formation by the Transcription Factor XBP1. *Cell Rep.* 2016;14(6):1382–1394.
36. Cao L et al. VEGF links hippocampal activity with neurogenesis, learning and memory. *Nat Genet.* 2004;36(8):827–835.
37. Mews P et al. Acetyl-CoA synthetase regulates histone acetylation and hippocampal memory. *Nature* 2017;546(7658):381–386.
38. Jacobson KA, von Lubitz DK, Daly JW, Fredholm BB. Adenosine receptor ligands: differences with acute versus chronic treatment. *Trends Pharmacol Sci.* 1996;17(3):108–113.
39. Ferré S. An update on the mechanisms of the psychostimulant effects of caffeine. *J Neurochem.* 2008;105(4):1067–1079.
40. Doepker C et al. Caffeine: Friend or Foe? *Annu Rev Food Sci Technol.* 2016;7:117–137.
41. Yu L et al. Uncovering multiple molecular targets for caffeine using a drug target validation strategy combining A2A receptor knockout mice with microarray profiling. *Physiol Genomics* 2009;37(3):199–210.
42. Svenningsson P, Nomikos GG, Fredholm BB. The stimulatory action and the development of tolerance to caffeine is associated with alterations in gene expression in specific brain regions. *J Neurosci.* 1999;19(10):4011–4022.
43. Magalhães R et al. Habitual coffee drinkers display a distinct pattern of brain functional connectivity. *Mol Psychiatry* 2021;26(11):6589–6598.
44. A. KK et al. TORC1 is a calcium- and cAMP-sensitive coincidence detector involved in hippocampal long-term synaptic plasticity. *Proc Natl Acad Sci.* 2007;104(11):4700–4705.
45. Chang D et al. Caffeine Caused a Widespread Increase of Resting Brain Entropy. *Sci Rep.* 2018;8(1):2700.
46. Tal O et al. Caffeine-Induced Global Reductions in Resting-State BOLD Connectivity Reflect Widespread Decreases in MEG Connectivity. *Front Hum Neurosci.* 2013;7:63.
47. Koppelstaetter F et al. Does caffeine modulate verbal working memory processes? An fMRI study. *Neuroimage* 2008;39(1):492–499.
48. Cunha RA. Different cellular sources and different roles of adenosine: A1 receptor-mediated inhibition through astrocytic-driven volume transmission and synapse-restricted A2A receptor-

mediated facilitation of plasticity. *Neurochem Int.* 2008;52(1–2):65–72.
49. Lopes L V, Cunha RA, Ribeiro JA. Cross talk between A(1) and A(2A) adenosine receptors in the hippocampus and cortex of young adult and old rats. *J Neurophysiol.* 1999;82(6):3196–3203.
50. Dassesse D, Ledent C, Parmentier M, Schiffmann SN. Acute and chronic caffeine administration differentially alters striatal gene expression in wild-type and adenosine A(2A) receptor-deficient mice. *Synapse* 2001;42(2):63–76.
51. Burns AM, Gräff J. Cognitive epigenetic priming: leveraging histone acetylation for memory amelioration. *Curr Opin. Neurobiol.* 2021;67:75–84.
52. Duarte JMN, Cunha RA, Carvalho RA. Adenosine A_1 receptors control the metabolic recovery after hypoxia in rat hippocampal slices. *J Neurochem.* 2016;136(5):947–957.
53. Laurent C et al. Beneficial effects of caffeine in a transgenic model of Alzheimer's disease-like tau pathology. *Neurobiol Aging* 2014;35(9):2079–2090.
54. Arendash GW et al. Caffeine protects Alzheimer's mice against cognitive impairment and reduces brain beta-amyloid production. *Neuroscience* 2006;142(4):941–952.
55. David B, V. LL. Stabilizing synapses. *Science.* 2021;374(6568):684–685.
56. G. SC et al. Adenosine Receptor Antagonists Including Caffeine Alter Fetal Brain Development in Mice. *Sci Transl Med.* 2013;5(197):197ra104-197ra104.
57. Ferran G-C et al. Convergence of adenosine and GABA signaling for synapse stabilization during development. *Science.* 2022;374(6568):eabk2055.
58. Arendash GW et al. Caffeine reverses cognitive impairment and decreases brain amyloid-beta levels in aged Alzheimer's disease mice. *J Alzheimers Dis.* 2009;17(3):661–680.
59. Laurent C et al. Beneficial effects of caffeine in a transgenic model of Alzheimer's disease-like tau pathology. *Neurobiol Aging* 2014;35(9):2079–2090.
60. Dobin A et al. STAR: ultrafast universal RNA-seq aligner. *Bioinformatics* 2013;29(1):15–21.
61. Langmead B, Salzberg SL. Fast gapped-read alignment with Bowtie 2. *Nat Methods* 2012;9(4):357–359.
62. Anders S, Pyl PT, Huber W. HTSeq--a Python framework to work with high-throughput sequencing data. *Bioinformatics* 2015;31(2):166–169.
63. Anders S, Huber W. Differential expression analysis for sequence count data. *Genome Biol.* 2010;11(10):R106.
64. Love MI, Huber W, Anders S. Moderated estimation of fold change and dispersion for RNA-seq data with DESeq2. *Genome Biol.* 2014;15(12):550.
65. Benjamini Y, Hochberg Y. Controlling the False Discovery Rate - a Practical and Powerful Approach to Multiple Testing. *J R Stat Soc Ser B-Methodological.* 1995;57(1):289–300.

66. Li H et al. The Sequence Alignment/Map format and SAMtools. *Bioinformatics* 2009;25(16):2078–2079.

67. Quinlan AR, Hall IM. BEDTools: a flexible suite of utilities for comparing genomic features. *Bioinformatics* 2010;26(6):841–842.

68. Xu S, Grullon S, Ge K, Peng W. Spatial clustering for identification of ChIP-enriched regions (SICER) to map regions of histone methylation patterns in embryonic stem cells. *Methods Mol Biol.* 2014;1150:97–111.

69. Zang C et al. A clustering approach for identification of enriched domains from histone modification ChIP-Seq data. *Bioinformatics* 2009;25(15):1952–1958.

70. Amemiya HM, Kundaje A, Boyle AP. The ENCODE Blacklist: Identification of Problematic Regions of the Genome. *Sci Rep.* 2019;9(1):9354.

71. Heinz S et al. Simple combinations of lineage-determining transcription factors prime cis-regulatory elements required for macrophage and B cell identities. *Mol Cell* 2010;38(4):576–589.

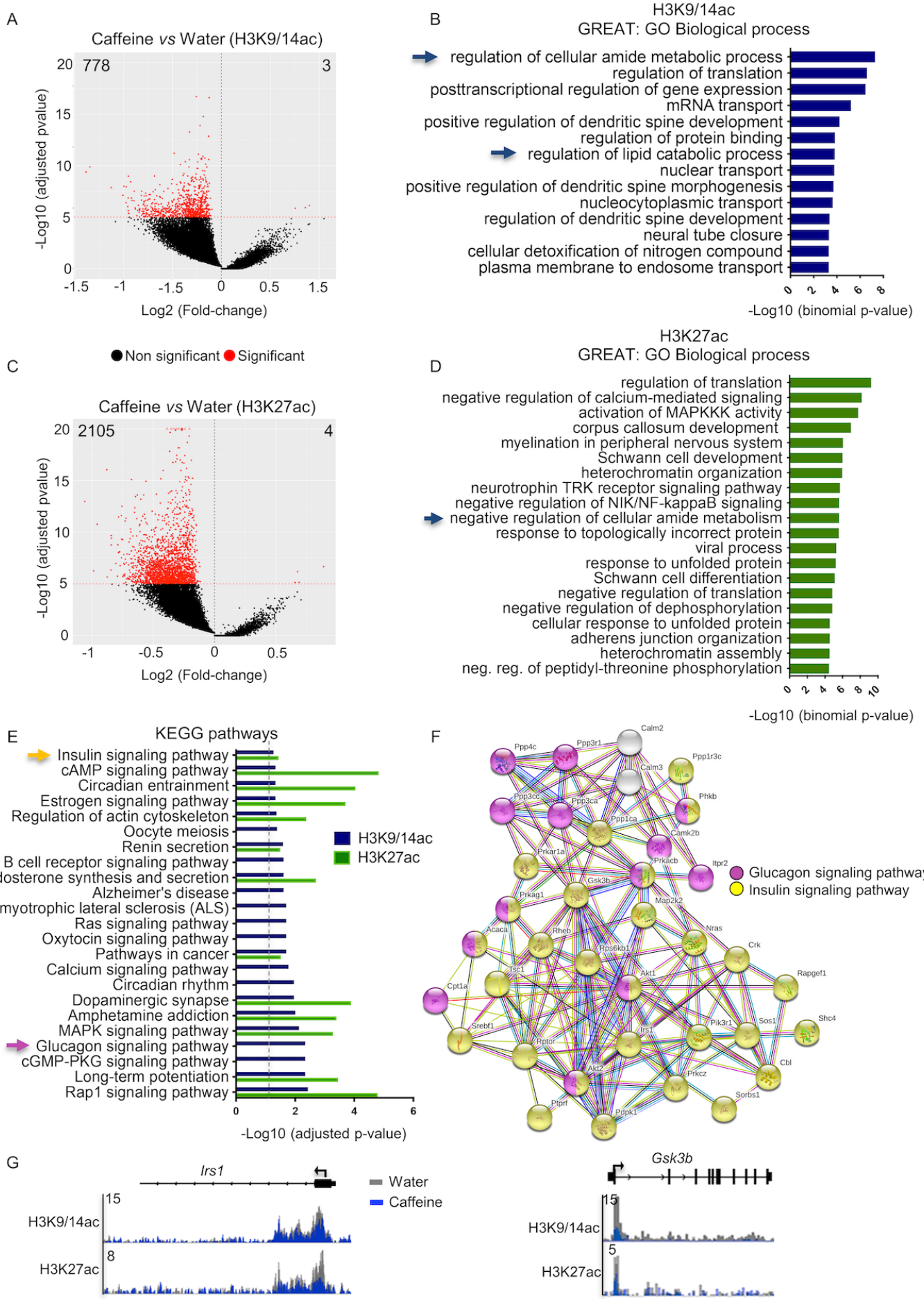
A
Caffeine vs Water (H3K9/14ac)
778
3
-Log10 (adjusted pvalue)
Log2 (Fold-change)
B
H3K9/14ac
GREAT: GO Biological process
regulation of cellular amide metabolic process
regulation of translation
posttranscriptional regulation of gene expression
mRNA transport
positive regulation of dendritic spine development
regulation of protein binding
regulation of lipid catabolic process
nuclear transport
positive regulation of dendritic spine morphogenesis
nucleocytoplasmic transport
regulation of dendritic spine development
neural tube closure
cellular detoxification of nitrogen compound
plasma membrane to endosome transport
-Log10 (binomial p-value)
Non significant
Significant
C
Caffeine vs Water (H3K27ac)
2105
4
-Log10 (adjusted pvalue)
Log2 (Fold-change)
D
H3K27ac
GREAT: GO Biological process
regulation of translation
negative regulation of calcium-mediated signaling
activation of MAPKKK activity
corpus callosum development
myelination in peripheral nervous system
Schwann cell development
heterochromatin organization
neurotrophin TRK receptor signaling pathway
negative regulation of NIK/NF-kappaB signaling
negative regulation of cellular amide metabolism
response to topologically incorrect protein
viral process
response to unfolded protein
Schwann cell differentiation
negative regulation of translation
negative regulation of dephosphorylation
cellular response to unfolded protein
adherens junction organization
heterochromatin assembly
neg. reg. of peptidyl-threonine phosphorylation
-Log10 (binomial p-value)
E
KEGG pathways
Insulin signaling pathway
cAMP signaling pathway
Circadian entrainment
Estrogen signaling pathway
Regulation of actin cytoskeleton
Oocyte meiosis
Renin secretion
B cell receptor signaling pathway
Aldosterone synthesis and secretion
Alzheimer's disease
Amyotrophic lateral sclerosis (ALS)
Ras signaling pathway
Oxytocin signaling pathway
Pathways in cancer
Calcium signaling pathway
Circadian rhythm
Dopaminergic synapse
Amphetamine addiction
MAPK signaling pathway
Glucagon signaling pathway
cGMP-PKG signaling pathway
Long-term potentiation
Rap1 signaling pathway
H3K9/14ac
H3K27ac
-Log10 (adjusted p-value)
F
Glucagon signaling pathway
Insulin signaling pathway
G
Irs1
Water
Caffeine
H3K9/14ac
H3K27ac
Gsk3b
H3K9/14ac
H3K27ac

Figure 1. Hippocampal epigenomic alterations associated with chronic caffeine consumption. (A) Volcano plot showing the differential enriched genomic regions of H3K9/14ac (ChIP-seq) upon chronic caffeine treatment (778 decreased and 3 increased peaks). Red dots represent the significant different regions (FDR<1E-5). (B) Genomic Regions Enrichment of Annotations Tool (GREAT) analysis showing the most enriched biological processes associated with the H3K9/14ac decreased peaks in caffeine-treated mice. Blue arrows point towards metabolic processes and translation related terms. (C) Volcano plot representing the differentially regulated regions of H3K27ac upon chronic caffeine treatment (2105 decreased and 4 increased peaks, with FDR<1E-5). (D) GREAT analysis representing the most common biological processes associated with the H3K27ac decreased peaks in the caffeine group. Regulation of metabolic processes are indicated by the blue arrows. (E) KEGG pathway analyses of depleted regions of both histone marks. Dashed grey line indicates the significant adjusted p-value <0.05. (F) Functional protein-protein network analysis (STRING) representation of insulin and glucagon-related genes found decreased in both histone acetylation marks. (G) Representation of the genomic regions (IGV) of the metabolic genes *Irs1* and *Gsk3b* showing significant decrease of H3K27ac and H3K9/14ac after caffeine treatment (*Irs1* H3K27ac FDR=1.82E-12; H3K9/14ac FDR=7.75E-05; *Gsk3b* H3K27ac FDR=4.83E-05; H3K9/14ac FDR=2.58E-11). Two biological replicates per histone mark were used for ChIP-seq experiments.

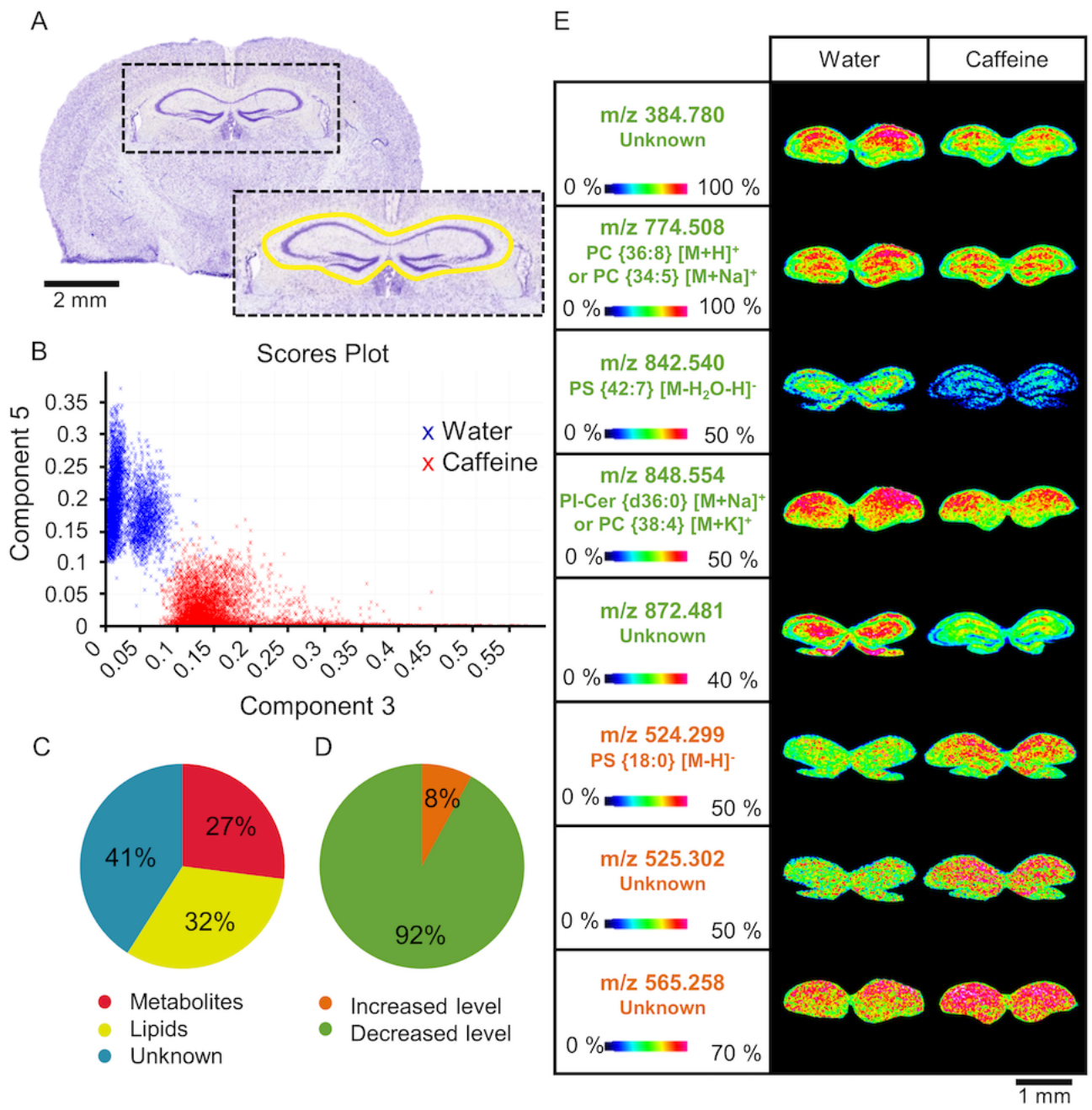
A
2 mm
B
Scores Plot
Component 5
Component 3
x Water
x Caffeine
C
27%
41%
32%
Metabolites
Lipids
Unknown
D
8%
92%
Increased level
Decreased level
E
Water
Caffeine
m/z 384.780
Unknown
0 %
100 %
m/z 774.508
PC {36:8} [M+H]+
or PC {34:5} [M+Na]+
0 %
100 %
m/z 842.540
PS {42:7} [M-H2O-H]-
0 %
50 %
m/z 848.554
PI-Cer {d36:0} [M+Na]+
or PC {38:4} [M+K]+
0 %
50 %
m/z 872.481
Unknown
0 %
40 %
m/z 524.299
PS {18:0} [M-H]-
0 %
50 %
m/z 525.302
Unknown
0 %
50 %
m/z 565.258
Unknown
0 %
70 %
1 mm

Figure 2. Hippocampal metabolomic changes induced by chronic caffeine consumption. Unsupervised principal component analysis (PCA) performed in the hippocampal region of interest delimitated in yellow on the Nissl staining of the brain tissue section (A). Scores from the unsupervised PCA in the hippocampus of Water- (in blue) and Caffeine-treated mice (in red) are presented in a plot where the differences between the molecular signatures of the two experimental groups clearly emerge (B). Pie charts showing the distribution of the different classes of molecules (C) and their abundance changes (D) of *m/z* measured in positive or negative ionization modes with a significant quantitative difference after the Student's *t*-test analysis in the hippocampus of Caffeine- compared to Water-treated animals (N = 6/group). (E) Mass spectrometry images obtained at a spatial resolution of 35 µm for *m/z* presenting a decreased (green) or increased (orange) density in the hippocampus of Caffeine-treated compared to Water-treated mice. The color scale shows the intensity of the *m/z* of interest. *Cer*, ceramide; *PC*, phosphatidylcholine; *PI*, phosphatidylinositol; *PS*, phosphatidylserine.

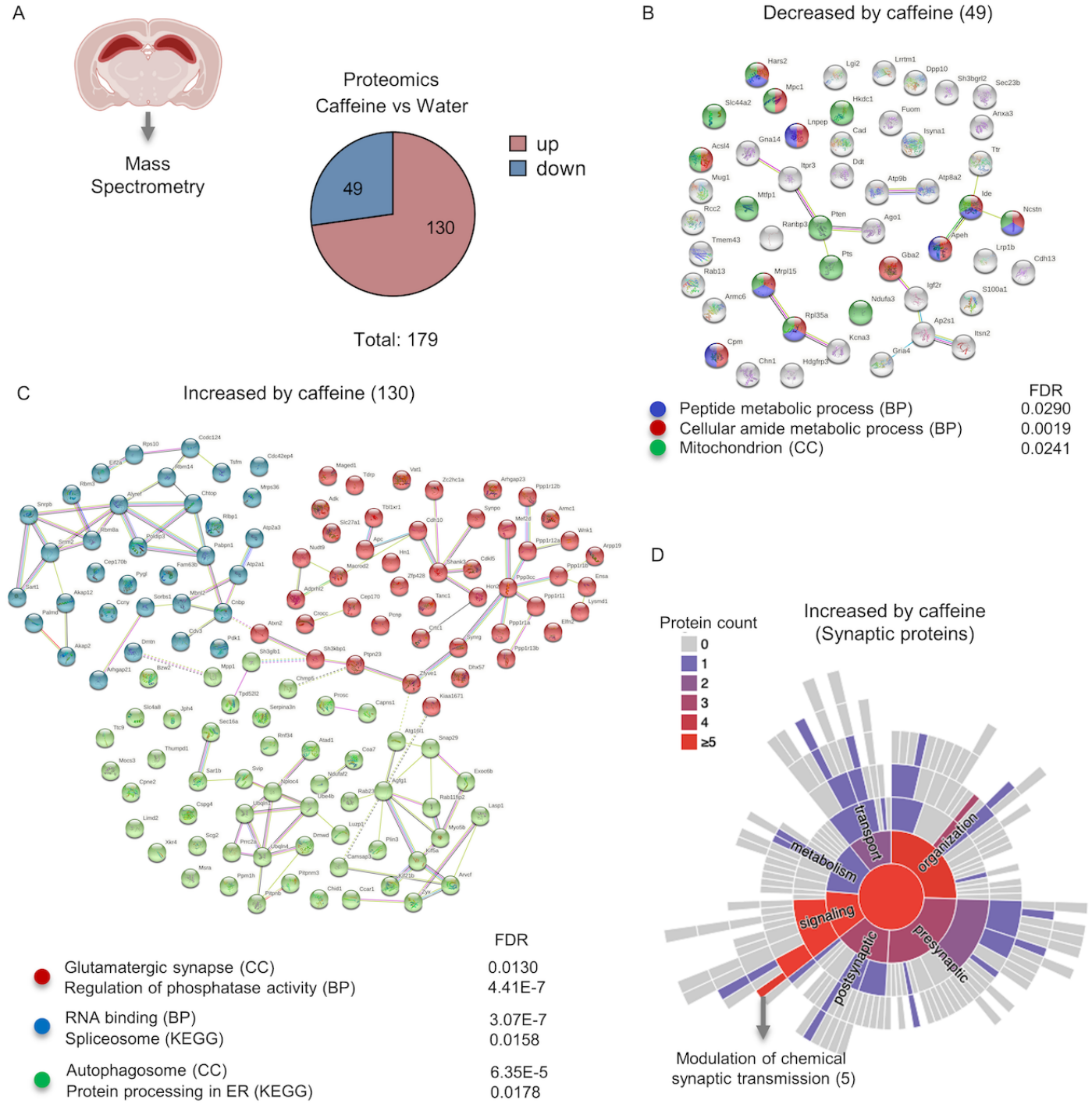
A
Mass
Spectrometry
Proteomics
Caffeine vs Water
49
130
up
down
Total: 179
B
Decreased by caffeine (49)
FDR
Peptide metabolic process (BP) 0.0290
Cellular amide metabolic process (BP) 0.0019
Mitochondrion (CC) 0.0241
C
Increased by caffeine (130)
FDR
Glutamatergic synapse (CC) 0.0130
Regulation of phosphatase activity (BP) 4.41E-7
RNA binding (BP) 3.07E-7
Spliceosome (KEGG) 0.0158
Autophagosome (CC) 6.35E-5
Protein processing in ER (KEGG) 0.0178
D
Protein count
0
1
2
3
4
≥5
Increased by caffeine
(Synaptic proteins)
transport
organization
metabolism
signaling
presynaptic
postsynaptic
Modulation of chemical
synaptic transmission (5)

Figure 3. Alteration of hippocampal proteomics induced by chronic caffeine consumption. (A) Pie-chart indicating proteins altered in the hippocampus of water and caffeine-treated mice determined by mass spectrometry analysis (N=3/group). In total 179 proteins were altered, of which 49 were decreased and 130 were increased by chronic caffeine. (B) STRING network analysis of the 49 decreased proteins in the caffeine condition showing that they were related to metabolic and mitochondrion related terms. (C) STRING network analysis of the 130 increased proteins by chronic caffeine revealing 3 major clusters (kmeans). The cluster in red shows significance for glutamatergic synapse-related terms, the blue cluster represents proteins associated with RNA binding and the green one autophagosome related-pathways. (BP-biological processes; CC-cellular component; KEGG: Kyoto Encyclopedia of Genes and Genomes). (D) Synaptic Gene Ontologies and annotations (SynGO, (26)) tool revealing that most of the synaptic proteins among the increased proteins by chronic caffeine are mostly associated with synaptic signaling and modulation of chemical synaptic transmission. Warmer colors represent predominance of proteins associated with the respective pathway.

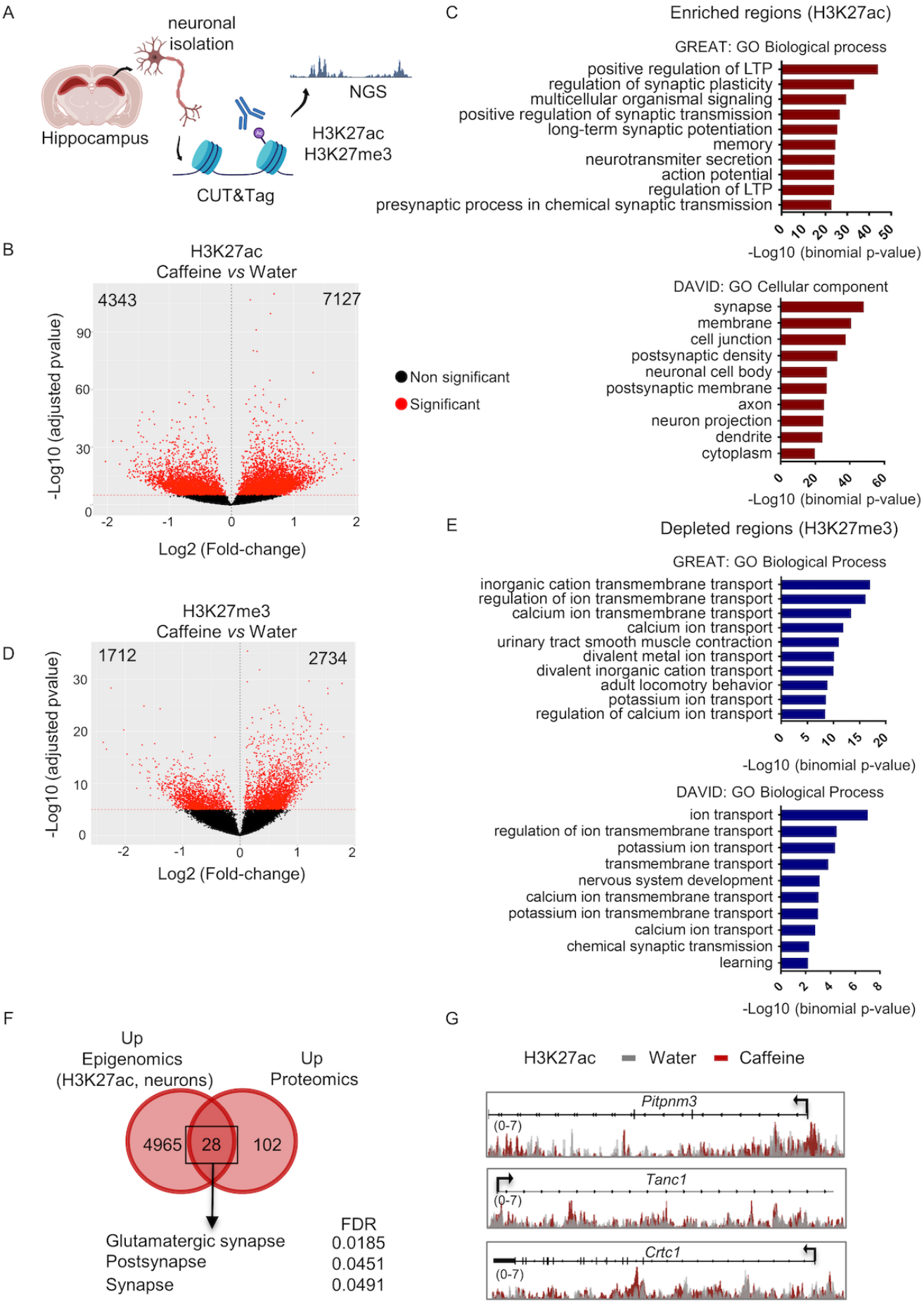
A
neuronal isolation
Hippocampus
NGS
H3K27ac
H3K27me3
CUT&Tag
B
H3K27ac
Caffeine vs Water
4343
7127
-Log10 (adjusted pvalue)
Log2 (Fold-change)
Non significant
Significant
C
Enriched regions (H3K27ac)
GREAT: GO Biological process
positive regulation of LTP
regulation of synaptic plasticity
multicellular organismal signaling
positive regulation of synaptic transmission
long-term synaptic potentiation
memory
neurotransmiter secretion
action potential
regulation of LTP
presynaptic process in chemical synaptic transmission
-Log10 (binomial p-value)
DAVID: GO Cellular component
synapse
membrane
cell junction
postsynaptic density
neuronal cell body
postsynaptic membrane
axon
neuron projection
dendrite
cytoplasm
-Log10 (binomial p-value)
D
H3K27me3
Caffeine vs Water
1712
2734
-Log10 (adjusted pvalue)
Log2 (Fold-change)
E
Depleted regions (H3K27me3)
GREAT: GO Biological Process
inorganic cation transmembrane transport
regulation of ion transmembrane transport
calcium ion transmembrane transport
calcium ion transport
urinary tract smooth muscle contraction
divalent metal ion transport
divalent inorganic cation transport
adult locomotry behavior
potassium ion transport
regulation of calcium ion transport
-Log10 (binomial p-value)
DAVID: GO Biological Process
ion transport
regulation of ion transmembrane transport
potassium ion transport
transmembrane transport
nervous system development
calcium ion transmembrane transport
potassium ion transmembrane transport
calcium ion transport
chemical synaptic transmission
learning
-Log10 (binomial p-value)
F
Up
Epigenomics
(H3K27ac, neurons)
Up
Proteomics
4965
28
102
FDR
Glutamatergic synapse 0.0185
Postsynapse 0.0451
Synapse 0.0491
G
H3K27ac
Water
Caffeine
Pitpnm3
Tanc1
Crtc1
(0-7)

Figure 4. **Neuronal-specific H3K27ac and H3K27me3 changes induced by chronic caffeine consumption.** (A) Schematics of the experimental design used to assess the active (H3K27ac) and repressive (H3K27me3) histone marks by CUT&Tag technique in an hippocampal neuronal-enriched population. (B) Volcano plot representing H3K27ac differentially regulated regions (4343 depleted and 7127 enriched, FDR<1E-5). (C, above) GREAT analysis showing the most enriched biological processes associated with the H3K27ac enriched peaks in caffeine-treated mice, mostly related to synaptic transmission. (C, below) DAVID Gene Ontology analysis revealing the most significant cellular components associated with H3K27ac enriched regions. (D) Volcano plot showing H3K27me3 differentially regulated regions between the water (control) and caffeine-treated mouse hippocampus (1712 depleted and 2734 enriched, FDR<1E-5). (E, above) GREAT analysis showing that depleted regions are mostly associated with ion transport processes. (E, below) DAVID Gene Ontology analysis indicating the most significant biological processes associated with H3K27ac enriched genes in neurons. (F) Venn diagram showing that 28 proteins were increased by caffeine and enriched in H3K27ac at their coding genes. These proteins are mostly associated with glutamatergic synapse (STRING analysis). (G) Representation of the genomic regions (IGV) of enriched H3K27ac genes by chronic caffeine in neurons. Two biological replicates per histone mark were used for CUT&Tag experiments.

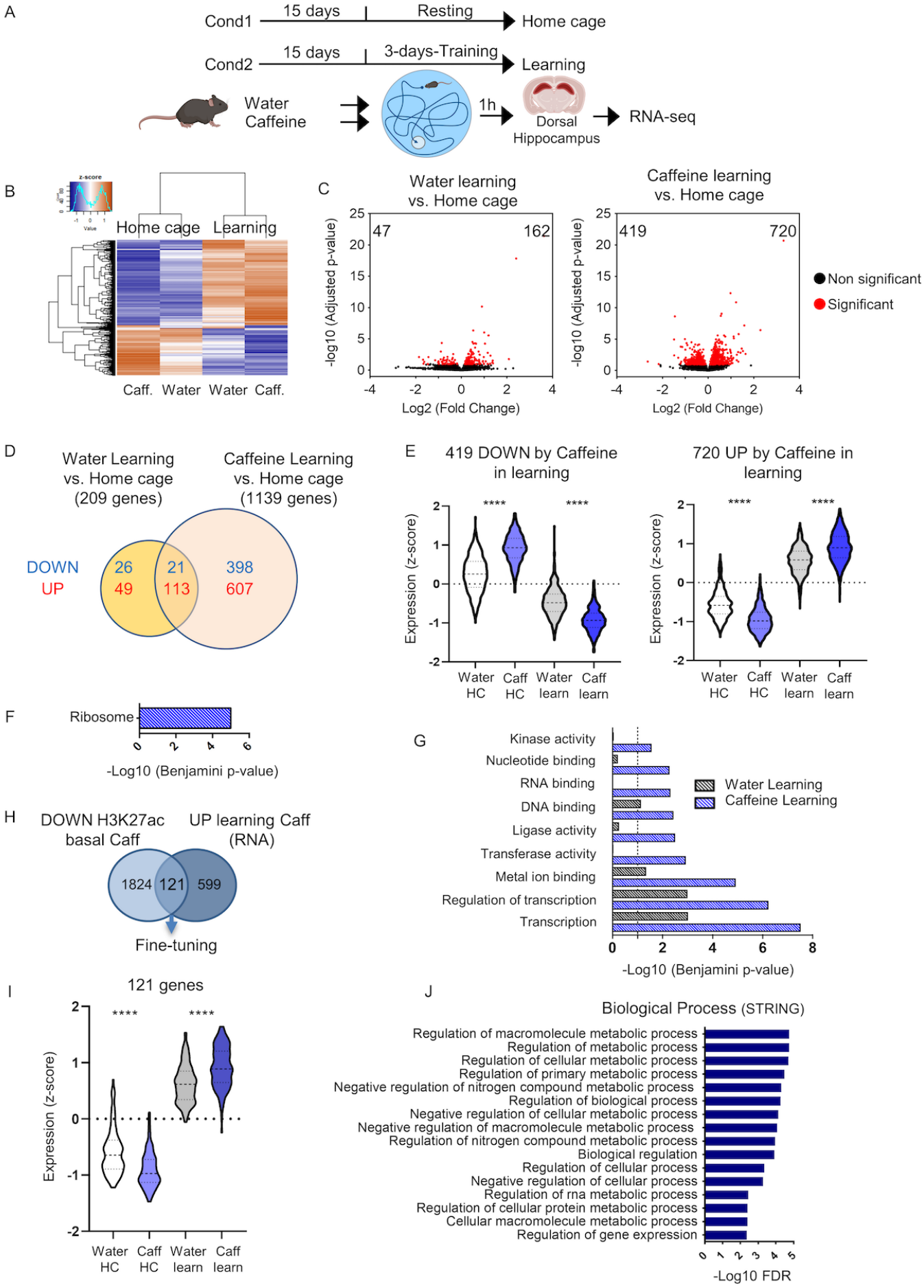
A
Cond1
15 days
Resting
Home cage
Cond2
15 days
3-days-Training
Learning
Water
Caffeine
1h
Dorsal
Hippocampus
RNA-seq
B
z-score
Home cage
Learning
Caff.
Water
Water
Caff.
C
Water learning
vs. Home cage
Caffeine learning
vs. Home cage
47
162
419
720
-log10 (Adjusted p-value)
Log2 (Fold Change)
Non significant
Significant
D
Water Learning
vs. Home cage
(209 genes)
Caffeine Learning
vs. Home cage
(1139 genes)
DOWN
UP
26
49
21
113
398
607
E
419 DOWN by Caffeine
in learning
720 UP by Caffeine in
learning
Expression (z-score)
****
Water
HC
Caff
HC
Water
learn
Caff
learn
F
Ribosome
-Log10 (Benjamini p-value)
G
Kinase activity
Nucleotide binding
RNA binding
DNA binding
Ligase activity
Transferase activity
Metal ion binding
Regulation of transcription
Transcription
Water Learning
Caffeine Learning
-Log10 (Benjamini p-value)
H
DOWN H3K27ac
basal Caff
UP learning Caff
(RNA)
1824
121
599
Fine-tuning
I
121 genes
Expression (z-score)
****
Water
HC
Caff
HC
Water
learn
Caff
learn
J
Biological Process (STRING)
Regulation of macromolecule metabolic process
Regulation of metabolic process
Regulation of cellular metabolic process
Regulation of primary metabolic process
Negative regulation of nitrogen compound metabolic process
Regulation of biological process
Negative regulation of cellular metabolic process
Negative regulation of macromolecule metabolic process
Regulation of nitrogen compound metabolic process
Biological regulation
Regulation of cellular process
Negative regulation of cellular process
Regulation of rna metabolic process
Regulation of cellular protein metabolic process
Cellular macromolecule metabolic process
Regulation of gene expression
-Log10 FDR

Figure 5. Hippocampal transcriptomic alterations induced by chronic caffeine consumption in learning conditions. (A) Experimental procedure of the RNA-seq experiments in home cage and learning groups. After chronic caffeine consumption (or water as a control), mice were subjected to 3 days training in Morris Water Maze and dorsal hippocampus was dissected 1h after the last trial for RNA-seq. (B) Heatmap representation of RNA-seq results (z-score) between the four groups. A total of 4 biological replicates were used per group. Color coding was performed according to the z-score of the normalized reads counts divided by gene length. (C, left) Volcano plots showing the differentially expressed hippocampal genes (adjusted *p*-value < 0.1) between Control learning *vs*. Control Home cage. (C, right) Volcano plot showing Caffeine-treated mice learning *vs.* Caffeine home cage differentially expressed genes (adjusted *p*-value < 0.1). (D) Venn diagrams showing the transcriptome changes induced by learning in Water and Caffeine animals (adjusted *p*-value < 0.1). (E) Violin plots representing the expression values (z-score) of the 419 genes downregulated and the 720 upregulated by caffeine (caff) in learning (learn) showing opposite trend among the home cage (HC) groups. (F) KEGG pathways analysis showing that most of the downregulated genes by caffeine upon learning are associated with ribosome. (G) Functional annotation performed with DAVID and their significance for the effect of learning in either water (black dashed bars) and Caffeine-treated animals (blue dashed bars). (H) Venn diagram revealing 121 genes depleted in H3K27ac (bulk hippocampus ChIP-seq) and up-regulated (RNA-seq) by learning in caffeine-treated mice. (I) Violin plots of the expression values (z-score) of the 121 genes. (J) Gene ontology analysis performed with STRING of the 121 genes showing a strong association with metabolic related biological processes (top 16 by FDR). Statistical significance in E and I were calculated by one-way ANOVA followed by Bonferroni's multiple comparison post hoc test;****$p<0.0001$.